Cellular and Molecular Life Sciences (2021) 78:2929–2948
https://doi.org/10.1007/s00018-020-03683-9

ORIGINAL ARTICLE

Macrophage ubiquitin-specific protease 2 contributes to motility, hyperactivation, capacitation, and in vitro fertilization activity of mouse sperm

Mayuko Hashimoto[1] · Shunsuke Kimura[3] · Chihiro Kanno[4] · Yojiro Yanagawa[4] · Takafumi Watanabe[2] · Jun Okabe[5] · Eiki Takahashi[6] · Masashi Nagano[7] · Hiroshi Kitamura[1]

Received: 17 May 2020 / Revised: 15 September 2020 / Accepted: 9 October 2020 / Published online: 26 October 2020

Abstract

Macrophages are innate immune cells that contribute to classical immune functions and tissue homeostasis. Ubiquitin-specific protease 2 (USP2) controls cytokine production in macrophages, but its organ-specific roles are still unknown. In this study, we generated myeloid-selective *Usp2* knockout (ms*Usp2*KO) mice and specifically explored the roles of testicular macrophage-derived USP2 in reproduction. The ms*Usp2*KO mice exhibited normal macrophage characteristics in various tissues. In the testis, macrophage *Usp*2 deficiency negligibly affected testicular macrophage subpopulations, spermatogenesis, and testicular organogenesis. However, frozen–thawed sperm derived from ms*Usp2*KO mice exhibited reduced motility, capacitation, and hyperactivation. In addition, macrophage *Usp2* ablation led to a decrease in the sperm population exhibiting high intracellular pH, calcium influx, and mitochondrial membrane potential. Interrupted pronuclei formation in eggs was observed when using frozen–thawed sperm from ms*Usp2*KO mice for in vitro fertilization. Administration of granulocyte macrophage-colony stimulating factor (GM-CSF), whose expression was decreased in testicular macrophages derived from ms*Usp2*KO mice, restored mitochondrial membrane potential and total sperm motility. Our observations demonstrate a distinct role of the deubiquitinating enzyme in organ-specific macrophages that directly affect sperm function.

Keywords USP · Granulocyte macrophage-colony stimulating factor · Myeloid cells · Capacitation · Male sterility

Abbreviations

ALDH1A2	Aldehyde dehydrogenase 1a2
ALH	Amplitude of lateral head displacement
Ar	Androgen receptor
BCF	Beat-cross frequency
BSA	Bovine serum albumin
CASA	Computer-assisted sperm motility analysis
CSF1R	Colony-stimulating factor 1 receptor
CSF2Rα	Colony-stimulating factor 2 receptor α chain
CTC	Chlortetracycline
DDX	DEAD-box helicase
FACS	Fluorescence-activated cell sorting
GM-CSF	Granulocyte macrophage-colony stimulating factor
HSD3B	3-β-Hydroxysteroid dehydrogenase

Electronic supplementary material The online version of this article (https://doi.org/10.1007/s00018-020-03683-9) contains supplementary material, which is available to authorized users.

✉ Hiroshi Kitamura
ktmr@rakuno.ac.jp

[1] Laboratory of Veterinary Physiology, Department of Veterinary Medicine, School of Veterinary Medicine, Rakuno Gakuen University, Ebetsu, Japan

[2] Laboratory of Veterinary Anatomy, Department of Veterinary Medicine, School of Veterinary Medicine, Rakuno Gakuen University, Ebetsu, Japan

[3] Division of Biochemistry, Faculty of Pharmacy and Graduate School of Pharmaceutical Science, Keio University, Tokyo, Japan

[4] Laboratory of Theriogenology, Department of Veterinary Clinical Sciences, Graduate School of Veterinary Medicine, Hokkaido University, Sapporo, Japan

[5] Department of Diabetes, Central Clinical School, Faculty of Medicine, Nursing and Health Sciences, Monash University, Melbourne, Australia

[6] Research Resources Centre, RIKEN Brain Science Institute, Wako, Japan

[7] Laboratory of Animal Reproduction, Department of Animal Science, School of Veterinary Medicine, Kitasato University, Towada, Japan

Hvcn1	Voltage-gated hydrogen channel1
IL	Interleukin
iNOS	Inducible nitric oxide synthase
IVF	In vitro fertilization
KD	Knockdown
KO	Knockout
Lhcgr	Luteinizing hormone receptor
LyzM-Cre	B6.129P2-*Lyzs*$^{tm1(cre)Ifo}$
M-CSF	Macrophage-colony stimulating factor
MCT	Monocarboxylate transporter
MHCII	Major histocompatibility complex class II
MMP	Mitochondrial membrane potential
OXPHOS	Oxidative phosphorylation
PI	Propidium iodide
Q-FISH	Quantitative-fluorescent in situ hybridization
qRT-PCR	Quantitative reverse transcription-polymerase chain reaction
R26GRR	C57BL/6 N-Gt(ROSA)26Sor$^{tm1(CAG}$–EGFP,tdsRed)Utr/Rbrc
RDH10	Retinol dehydrogenase 10
Slc9c1	Solute carrier family 9 member C1
Sox	Sex-determining region Y-box transcription factor
Stra8	Stimulated by retinoic acid 8
TMB	3,3′,5,5′-Tetramethylbenzidine
TNF	Tumor necrosis factor
TREM	Tetramethylrhodamine methyl ester
USP	Ubiquitin-specific protease
VCL	Curvilinear velocity
VSL	Straight-line velocity

Introduction

Macrophages belong to the myeloid lineage of hematopoietic cells and have a wide variety of roles in maintaining homeostasis in various tissues [1–3]. Macrophages can be classified based on functional properties and the expression pattern of surface markers. Classically activated M1 macrophages exhibit a proinflammatory phenotype, while alternatively activated M2 macrophages have an anti-inflammatory phenotype, and they are characterized by the surface markers CD206^{-}/CD163^{-}/CD11c^{+}/Ly6c^{high}/inducible nitric oxide synthase (iNOS)$^{+}$/arginase^{-} and CD206^{+}/CD163^{+}/CD11c^{-}/Ly6c^{int}/iNOS^{-}/arginase^{+}, respectively [4–6]. In the testis, macrophages comprise one of the major cellular populations in the interstitial regions, almost one-fourth the number of Leydig cells [7]. Most testicular macrophages display the M2-type phenotype and contribute to the maintenance of the immune-privileged tissue environment and the elimination of apoptotic cells [7, 8]. De Falco et al. have demonstrated that testicular macrophages can be categorized into two distinct populations according to location and surface markers [9]. Interstitial macrophages, located adjacent to Leydig cells in the interstitial regions between seminiferous tubules, intensely express colony-stimulating factor 1 receptor (CSF1R) and MER receptor tyrosine kinase [9, 10]. In contrast, peritubular macrophages line seminiferous walls and abundantly express major histocompatibility complex class II (MHCII) [9]. Interstitial macrophages are derived from both the yolk sac and bone marrow, while peritubular macrophages are specifically derived from bone marrow [10]. Despite these pioneer studies, the detailed functions of interstitial and peritubular macrophages have not yet been fully elucidated.

In addition to the phagocytosis of cellular debris and foreign substances, macrophages also secrete various humoral factors that modulate immune responses, tissue development, tissue remodeling, and disease progression [11]. In the testis, macrophages participate in steroidogenesis and spermatogenesis, possibly via the production of several mediators. Deprivation of macrophages caused by liposome-entrapped dichloromethylene diphosphonate administration or macrophage-colony stimulating factor (M-CSF) deficiency can lead to developmental defects in Leydig cells and/or reduced spermatogenesis [12–14]. In addition, the diphtheria-inducible transient deletion of testicular macrophages using the *Cx3Cr1*-Cre; *Rosa*-iDTR system resulted in a substantial decrease in the number of spermatogonial precursors [9]. To date, various studies have identified that cytokines mediate signals from testicular macrophages to other gonadal cells (e.g., spermatocytes, Leydig cells, and Sertoli cells), especially in the context of inflammation. For instance, interleukin (IL)-1, IL-6, and tumor necrosis factor (TNF) from activated testicular macrophages modulate steroidogenesis in Leydig cells and spermatogenic cell differentiation [15, 16]. Other reports have sought to identify the function of testicular macrophage-derived factors in the testis during steady-state. For instance, M-CSF, which stimulates self-renewal of spermatogonial stem cells [17], is expressed in both interstitial and peritubular macrophages, as well as in other cell types, including myoid cells and vascular smooth muscle cells [9]. Moreover, the same report also indicated that testicular macrophages express two essential enzymes for retinoic acid synthesis, namely aldehyde dehydrogenase 1a2 (ALDH1A2) and retinol dehydrogenase 10 (RDH10) [9]. Further, other groups have demonstrated that rat testicular macrophages highly express granulocyte macrophage-colony stimulating factor (GM-CSF) [18], which has been found to maintain the motility of frozen–thawed sperm [19].

Mammalian fertilization is an intricate process, where male gametes undergo maturation and activation in anatomically distinct locations. Sperm gain the capacity for activation processes in the male genital tract, but the activation processes themselves, namely capacitation, hyperactive motility, and the acrosome reaction, occur in the female

genital tract. To perform the well-organized activation process, sperm gain energy from ATP, which is produced by both glycolysis and oxidative phosphorylation (OXPHOS). Therefore, intracellular ATP content can be considered a determinant of sperm activation [20]. OXPHOS has been shown to be responsible for total sperm motility, while glycolysis predominantly contributes to hyperactive progressive motility, capacitation, and the acrosome reaction [20]. Fueled by local glycolytic ATP production in the principal piece, hyperactive sperm are characterized by high amplitude and asymmetrical flagellar bending, with curvilinear motility [20, 21]. Capacitation and hyperactivation are initiated by cholesterol efflux at the plasma membrane, and are followed by intracellular alkalization [22]. Intracellular alkalization opens the CatSper, a sperm-specific calcium channel, which evokes transient calcium ion influx [22]. Moreover, calcium from intracellular organelles has also been postulated to participate in sperm hyperactivation [20–23]. Calcium is necessary for fertilization, as evidenced by a study showing that missense mutations of the *CatSper* genes result in infertility caused by aberrant sperm activation [23].

Ubiquitination and deubiquitination are reversible processes that affect the digestion and functional modulation of a target protein [24]. The degree of ubiquitination on target proteins is determined by the balance of ubiquitin ligase activity and ubiquitin protease activity. Ubiquitin-specific protease 2 (USP2), which is expressed in a wide variety of cells, has regulatory roles in various cellular functions, such as cell cycle progression [25] and cell death [26, 27]. USP2 has also been postulated to be a key modulator of higher-order functions in mammals, such as the maintenance of energy homeostasis [28–31] and special memory retrieval [32]. Our team and others have previously demonstrated that macrophage USP2 modulates the production of various cytokines [29, 33–35]. In bacterial lipopolysaccharide-activated macrophages, USP2 attenuates the production of proinflammatory cytokines, such as IL-6, IL-8, and TNF-α, by controlling the DNA binding ratio of the homeodomain proteins Oct-1 to Oct-2 to the respective *cis*-regulating elements of the cytokine gene [34]. In normal culture conditions, USP2 also modulates the production of several chemokines, such as the CC chemokine ligands 2, 4, and 24 in macrophage-like HL-60 cells [29]. These observations imply that USP2 is a regulatory molecule that maintains tissue homeostasis through cytokine production.

USP2 is believed to have a crucial role in spermatogenesis because it is exclusively expressed in late elongating spermatids [36]. In agreement with this idea, a previous report has demonstrated that *Usp2* knockout (KO) mice exhibited male sterility, with the *Usp2*KO sperm displaying severe defects in motility [37]. However, the biological role of USP2 in other testicular cells has not been investigated. In light of the critical role of testicular macrophages in male fertility, we used a myeloid-specific gene knockout mouse model in the present study to evaluate the modulatory roles of macrophage USP2 in testicular function.

Materials and methods

Mice

C57BL/6 mice were purchased from Japan SLC (Hamamatsu, Japan). B6.129P2-*Lyzs*$^{tm1(cre)Ifo}$ (*LyzM-Cre*) mice and C57BL/6N-Gt(ROSA)26Sor$^{tm1(CAG-EGFP,tdsRed)Utr/Rbrc}$ (R26GRR) mice were obtained from the RIKEN BioResource Research Center (Tsukuba, Japan) [38, 39]. For the construction of *Usp2*$^{fl/fl}$ mice, the *lox*P-*Neo*-*Usp2* exon 3–4-*lox*P cassette was inserted into the C57BL/6-derived embryonic stem cell genome. R26GRR/*LyzM-Cre* mice were generated by crossing R26GRR mice with *LyzM-Cre* mice. For the generation of myeloid-selective *Usp2* knockout (ms*Usp2*KO) mice, we first mated *Usp2*$^{fl/fl}$ mice with *LyzM-Cre* mice. Subsequently, we crossed *Usp2*$^{fl/+}$/*LyzM-Cre* offspring with *Usp2*$^{fl/fl}$ mice to generate *Usp2*$^{fl/fl}$/*LyzM-Cre* mice (ms*Usp2*KO). The mice were housed under conventional conditions at 24 ± 2 °C on a 12-h light–dark cycle (lights on from 8:00–20:00) and were given free access to food and water. Male mice aged 8–14 weeks were used for analyses. For tissue sampling, mice were anesthetized with pentobarbital sodium (200 mg/kg ip) and then killed by cervical dislocation.

Genotyping

The macrophage-abundant peritoneal cell fraction was prepared according to a previous manual [40]. Total RNA isolated with RNAiso plus (Takara Bio, Otsu, Japan) was subjected to reverse transcription using M-MLV reverse transcriptase (Nippon Gene, Tokyo, Japan) according to the manual. Genomic DNA was isolated using the KAPA Mouse Genotyping kit (KAPA Biosystems, Woburn, MA, USA). Subsequently, cDNA and genomic DNA were subjected to PCR analysis using Go*Taq* (Promega, Madison, WI, USA) and the primers as shown in Supplementary Table 1.

Histological analyses

To prepare cryosections, tissues were fixed with 4% paraformaldehyde overnight and then immersed in 30% sucrose. The tissues were then embedded in O.C.T. compound (Sakura Finetek, Tokyo, Japan) in liquid nitrogen and sectioned into 14 µm-thick slices. After removing the O.C.T. compound with phosphate-buffered saline (PBS), the tissue sections from R26GRR/ *LyzM-Cre* mice were subjected to

microscopic observation using a FV1000 confocal microscope (Olympus, Tokyo, Japan).

For immunohistochemical staining of the cryosections (Figs. 2d–g, 3a, 7g, and Supplementary Fig. 6), the goat serum-blocked cryosections were reacted with the primary antibodies listed in Supplementary Table 2, followed by incubation with biotin-conjugated anti-rabbit IgG (Jackson Immunoresearch, West Grove, PA, USA). Subsequently, the sections were reacted with the avidin–peroxidase complex (Nichirei, Tokyo, Japan). To detect antigen–antibody reactions, the sections were treated with 0.01% 3,3′-diaminobenzidine and 0.001% hydrogen peroxide in 10 mM Tris–HCl buffer (pH 7.6) and viewed using a BX-51 microscope connected to the DP27 camera (Olympus).

For immunofluorescent imaging of the cryosections (Fig. 1d and Supplementary Figs.1b–e, 4 and 5), 10% non-immunized goat serum-blocked cryosections were reacted overnight with the primary antibodies listed in Supplementary Table 2 overnight at 4 °C. Subsequently, the sections were reacted with either the Cy3-conjugated anti-rat IgG, Cy5-conjugated anti-rat IgG (Jackson Immunoresearch), or Alexa Fluor 488-conjugated anti-rabbit IgG (Thermo Fisher Scientific) at room temperature for 2 h. The nuclei were stained with SYTOX-Green (Thermo Fisher Scientific). The sections were afterward observed using an FV1000 microscope.

For immunohistochemical or immunofluorescent imaging of GM-CSF and macrophage markers in paraffin sections (Fig. 7c, Supplementary Figs. 10a, b, 11a, b, c), tissues were fixed with 4% paraformaldehyde at 4 °C overnight, embedded in paraffin wax according to the standard procedure, and sectioned at 3 µm. After deparaffinization, the sections were immersed in HistoVT One solution (Nacalai, Kyoto, Japan) at 90 °C for 20 min. To inactivate endogenous peroxidase, some sections were incubated in 0.3% hydrogen peroxide for 20 min. The sections were then treated with Blocking One Histo (Nacalai) at room temperature for 10 min and reacted with biotin-conjugated rat anti-mouse F4/80 antibody (Biolegend, San Diego, CA, USA) or rabbit anti-mouse GM-CSF antibody (Abcam) in 0.2% bovine serum albumin (BSA) containing PBS or Can Get Signal immunostain solution (Toyobo, Osaka, Japan) at 4 °C overnight. For immunofluorescent detection of GM-CSF and macrophage markers, the sections were treated with Alexa Fluor 488-conjugated anti-rabbit IgG (Thermo Fisher Scientific) and Alexa Fluor 555-conjugated streptavidin (Thermo Fisher Scientific), and mounted with Prolong Diamond with DAPI (Thermo Fisher Scientific). The sections were viewed using a C2 laser confocal microscope (Nikon, Tokyo, Japan). For chromogenic detection of GM-CSF, the GM-CSF antigen–antibody immunocomplex was visualized using the Histofine Simple Stain kit (Nichirei Bioscience), according to the manufacturer's instructions. The chromogenic signal was monitored using a BX50 microscope (Olympus). To determine the specificity of the anti-GM-CSF antibody, we preincubated the antibody with an excess amount of recombinant GM-CSF (GeneTex,

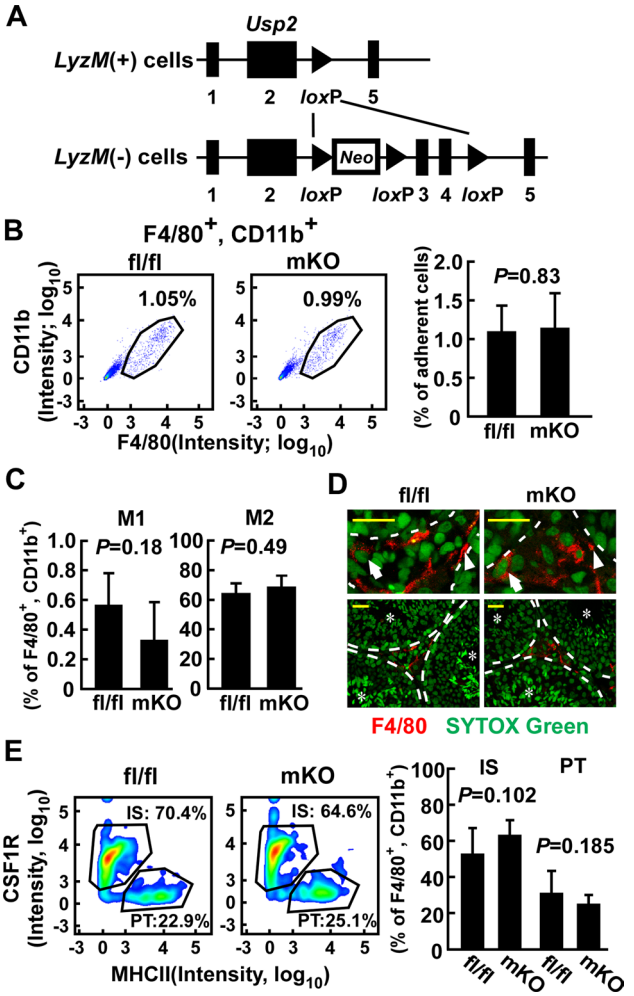

Fig. 1 Effect of myeloid-selective *Usp2* knockout on the proportion of the macrophage subpopulation in the testis. **a** Schematic presentation of the *Usp2* locus of *LyzM* (+) and (−) cells. Exon numbers and *lox*P sites are shown. *Neo* represents the neomycin-resistant gene. **b-e**: Myeloid-selective *Usp2* knockout mice (mKO) and *Usp2*$^{fl/fl}$ mice (fl/fl) were subjected to FACS analysis (**b**, **c**, **e**) and histological analysis (**d**). **b** The proportion of F4/80$^+$, CD11b$^+$ macrophages in the testicular adherent cell fraction. Representative flow cytometry scatter plots (left panels) and quantification of the macrophages (right panel) are shown. **c** Proportion of Ly6c^{high}, CD206$^-$ M1 macrophages (left) and Ly6c^{int}, CD206$^+$ M2 macrophages (right) in F4/80$^+$, CD11b$^+$ cells. **d** Representative images of interstitial (arrows) and peritubular (arrowheads) macrophages in the testis that were stained with an anti-F4/30 antibody. The top panels show an enlarged view of the bottom panels. Seminiferous tubules are shown by dashed lines and asterisks. Scale bars represent 20 µm. Data were reproducibly obtained from three individual mice. **e** The proportion of CSF1R$^+$, MHCII$^-$ interstitial (IS) and CSF1R$^-$, MHCII$^+$ peritubular (PT) macrophages in F4/80$^+$, CD11b$^+$ cells. Representative flow cytometry scatter plots (left panels) and quantification of IS and PT macrophages (right panel) are shown. Data are shown as the means ± SD of five mice (**b**, **c**, **e**). *P* values are shown in each graph (**b**, **c**, **e**)

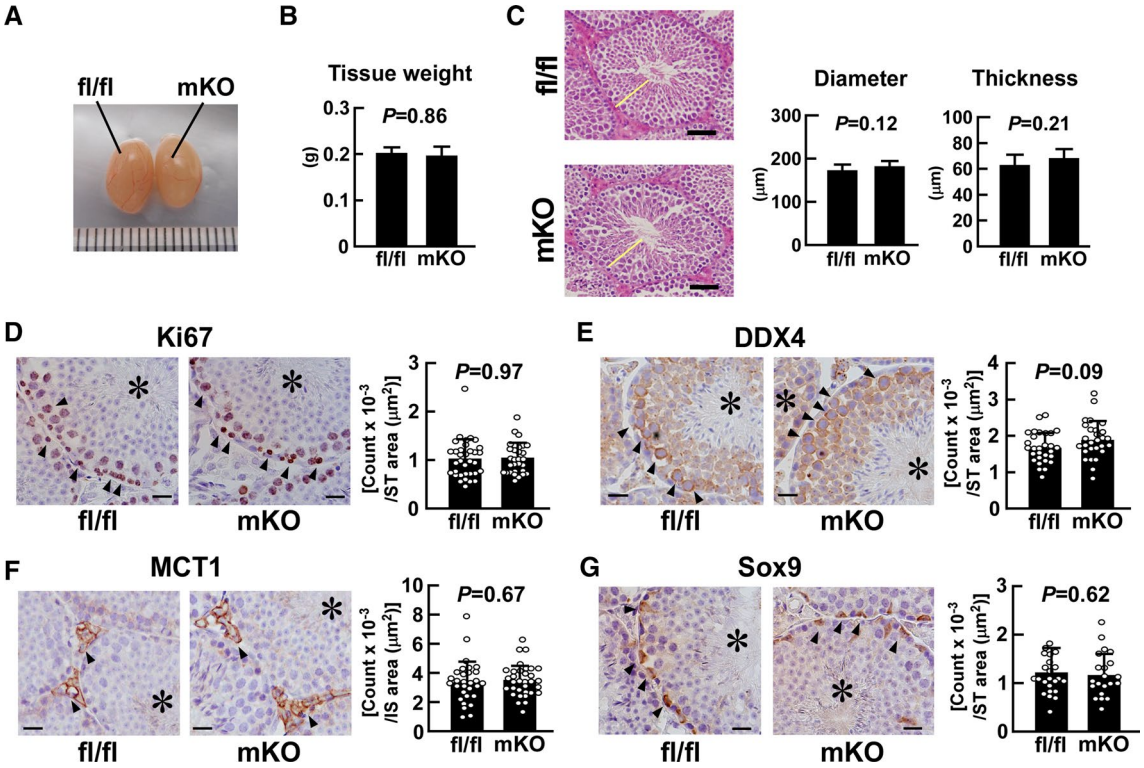

Fig. 2 Effect of myeloid-selective *Usp2* knockout on testicular organogenesis. **a**, **b** Morphology (**a**) and weight (**b**) of the testis in myeloid-selective *Usp2* knockout mice (mKO) and *Usp2*$^{fl/fl}$ mice (fl/fl). **c** The outer diameter and thickness of seminiferous tubules. Representative microscopic images (left panels) and quantification of their diameter and thickness (right panels). Yellow bars indicate the wall of the seminiferous tubules. The average thickness of the seminiferous tubule wall at four respective ends of the major and minor axes was calculated. **d–g** Immunohistochemical staining with antibodies against Ki67 (**d**), DDX4 (**e**), MCT1 (**f**), and Sox9 (**g**). Representative microscopic images and the density of immune-positive cells are shown in the left and right panels (**d–g**), respectively. Arrowheads indicate immunopositive cells, and asterisks show seminiferous tubules. Scale bars represent 20 μm. Immunopositive cells were counted in the seminiferous tubules (ST; **d, e**, **g**) or in the interstitial regions (IS; **f**) in five randomly selected microscopic fields for each individual. Data are shown as means ± SD of six (**b, c**) or five (**d–g**) mice, with counts of immunopositive cells in each area shown as dots. *P* values are shown in the graphs (**b–g**)

Irvine, CA, USA) in Can Get Signal immunostain solution at 4 °C overnight, and then applied the solution to the section as the first antibody.

Fluorescence-activated cell sorting (FACS) analysis of macrophage subpopulations

The testicular adherent cell fraction was prepared as previously described [41]. Briefly, the testis was cut into small pieces in a buffer containing 0.4 mg/mL collagenase (Sigma-Aldrich, St Louis, MI, USA) and 6 U/mL DNase I (New England Biolabs, Ipswich, MA, USA) and then incubated under vigorous agitation at 37 °C for 20 min. Cells attached to the dishes were subjected to FACS analysis. Splenocytes were prepared as previously described [42]. The cells were blocked with TruStain FcX (Biolegend) and labeled with the fluorescent dye-conjugated antibodies listed in Supplementary Table 2 at 4 °C for 1 h. After washing with PBS, the cells were monitored using FACSVerse (BD Biosciences, San Jose, CA, USA). FACS data were further analyzed using FlowJo software (FlowJo, Ashland, OR, USA).

Quantitative reverse transcription-polymerase chain reaction (qRT-PCR) analysis

cDNA was synthesized using M-MLV reverse transcriptase (Nippon Gene). A quantitative PCR was performed with the KAPA SYBR Fast qPCR kit (KAPA Biosystems) using an ECO qPCR system (Illumina, San Diego, CA, USA). The sequences of primers and hydrolysis probes used are listed in Supplementary Table 1. In some experiments, we performed cluster analysis using qRT-PCR data and generated heatmaps using the ClustVis program (https://biit.cs.ut.ee/clustvis/) [43]. Unit variance scaling, but not row centering, was applied to the heatmap rows.

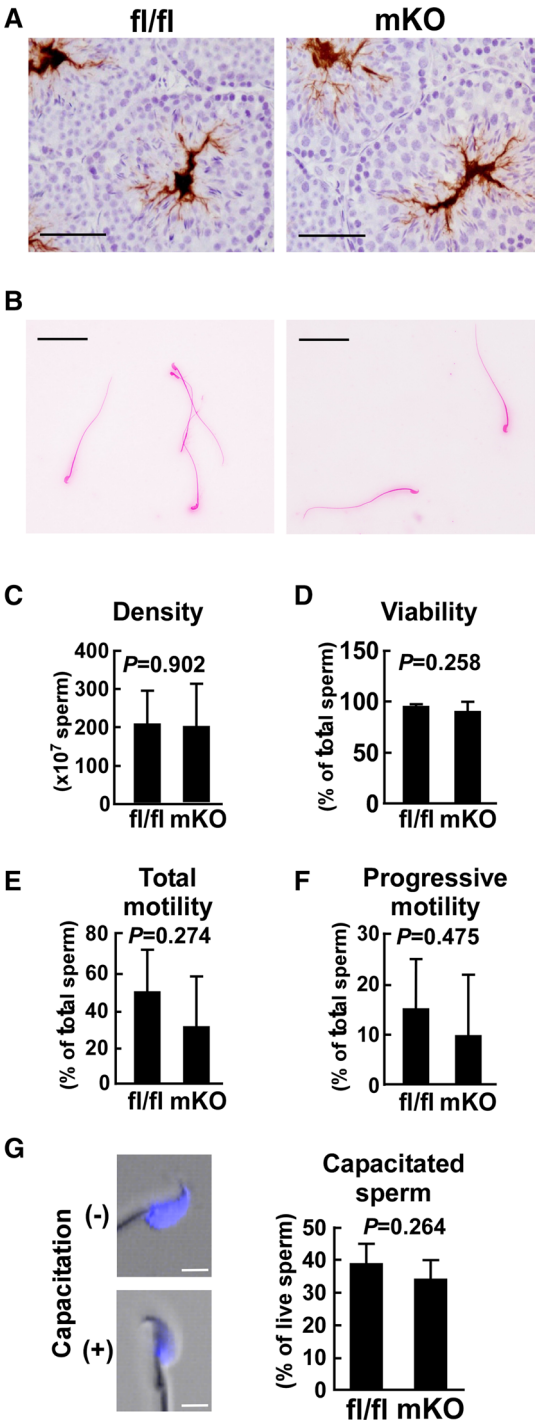

Fig. 3 Effect of myeloid-selective *Usp2* deficiency on the characteristics of freshly isolated sperm. **a** Representative histochemical images of mature sperm in the testis of myeloid-selective *Usp2* knockout mice (mKO) and *Usp2*$^{fl/fl}$ mice (fl/fl). The sperm were stained with an anti-MCT2 antibody. **b** The morphology of eosin-stained sperm from the epididymis. **c**, **d** The density (**c**) and viability (**d**) of the epididymal sperm. **e**, **f** Total (**e**) and progressive (**f**) sperm motility were evaluated by computer-assisted sperm motility analysis (CASA). **g** Representative images of chlortetracycline (CTC)-stained sperm (left) and capacitation rate in total sperm (right). Capacitated (+) and non-capacitated (-) sperm are shown. Scale bars represent 50 µm (**a, b**) or 5 µm (**g**). Reproducible histological data were obtained from three (**a**) or five (**b**, **g**) mice for each genotype. Data are shown as the means ± SD of 9–13 (**c**), 4–5 (**d**), 6 (**e**, **f**) or 5 (**g**) mice. Approximately, 300 (**e**, **f**) or 200 (**c**, **d**, **g**) sperm per mouse was used for the analysis. The *P* values are shown in graphs (**c–g**)

Testosterone concentration

The concentration of testosterone in serum and the testis was measured using a competitive double-antibody enzyme immunoassay that was described in a previous paper, with some modifications for testosterone [44]. Five µL of serum or frozen testis homogenate was diluted with 20 times volume of assay buffer (145 mM NaCl, 40 mM Na_2HPO_4, 0.1% BSA, pH 7.2). The diluent was then extracted using 20 times volume of diethyl-ether, and reconstituted with 100 µL of the assay buffer. Then, 20 µL samples were incubated with a 50 µL mixture of anti-testosterone-3E-CMO-BSA (FKA102; Cosmo Bio, Tokyo, Japan) and horseradish peroxidase-labeled testosterone (Sigma-Aldrich), in an anti-rabbit IgG (Jackson ImmunoResearch)-coated 96-well plate, for 16–18 h at 4 °C. After washing with 0.05% Tween 80, the plate was incubated with 150 µL of tetramethylbenzidine solution (1 mM 3,3′,5,5′-tetramethylbenzidine, 5 mM citric acid, 50 mM Na_2HPO_4, 500 mM urea hydrogen peroxide, 2% dimethyl sulfoxide) for 40 min at 37 °C. The chromogenic reaction was stopped with 50 µL of 4 N H_2SO_4. Absorbance at 450 nm was measured using a Model550 plate reader (Bio-Rad, Hercules, CA, USA). The detection limit was 19.5 pg/mL, and the intra- and inter-assay coefficients of variation were 4.8% and 13.0%, respectively.

Preparation of epididymal sperm

Sperm samples were isolated from the epididymis of ms*Usp2*KO mice and *Usp2*$^{fl/fl}$ mice. In some experiments, recombinant mouse GM-CSF (5 nM; GeneTex) or vehicle (0.4% BSA-containing PBS) was supplemented to the sperm in FERTIUP preincubation medium (Kyudo, Saga, Japan) for 30 min before freezing in liquid nitrogen until use. Before analysis, sperm (~ 5×10^6 per mouse) were incubated in 0.4% BSA-containing HTF medium for 60 min.

Sperm morphology and viability

Sperm were stained with 0.3% eosin Y solution (Muto, Tokyo, Japan) and 0.3% nigrosine solution (Wako) at room temperature for 1 min and smeared on a slide. The stained (dead) sperm were counted using the IX-71 microscope (Olympus); live sperm remained unstained. More than 200 total sperm were counted per individual. Mean sperm

viability was calculated as the proportion of live sperm in total sperm from 4–5 mice.

Computer-assisted sperm motility analysis (CASA)

Computer-assisted sperm motility analysis (CASA) was performed as previously described [45]. The freshly isolated or frozen–thawed collected sperm was subjected to an assessment of sperm motility using the SMAS system (DITECT, Tokyo, Japan). The SMAS system automatically calculated several kinetic parameters of the sperm. Sperm moving at more than 25 µm/s were regarded as "progressive motile" sperm. The number of sperm analyzed per sample was at least 300, including immotile sperm. To evaluate hyperactive sperm, we further analyzed the CASA data by K-means clustering, as described in a previous report [45]. Briefly, sperm was classified into four clusters using the K-means method, based on straight-line velocity (VSL) and curvilinear velocity (VCL). Clustering analysis was performed using the JMP14 software package (SAS institute, Cary, North Carolina, USA). The cluster containing sperm with high VCL and low linearity (LIN; determined by VSL/VCL) was defined as the hyperactive sperm cluster.

Chlortetracycline (CTC) assay

Capacitation was evaluated using an established CTC staining method, with minor modifications [46]. Briefly, sperm (5×10^5) from each mouse were prepared in 100 µL of modified Brackett–Oliphant medium and treated with bisbenzimide 33,258 (final concentration, 5 µg/mL) for 3 min. The sperm sample was then layered onto ten times volume of 3% polyvinylpyrrolidone (Sigma-Aldrich) in PBS and then centrifuged at 500×*g* for 5 min. The sperm were resuspended with 20 µL of CTC solution (375 µM CTC, 2.5 mM cysteine, 65 mM NaCl, 10 mM Tris–HCl, pH 7.8) and fixed with Tris–HCl-buffered (pH 7. 4) 1% paraformaldehyde. The sperm were smeared on a glass slide and viewed using an IX-71 microscope connected to the DP73 camera (Olympus). The heads of non-capacitated sperm were uniformly stained, while capacitated sperm exhibited restricted staining over the post-acrosome region. All reactions were performed at room temperature. A total of 200 sperm per mouse were used for CTC analysis.

Intracellular ATP content

After the sperm (~ 10,000 per mouse) were incubated in 50 µL of HTF medium at 37 °C for 90 min, an equal volume of the ATP measurement solution (Toyo B-Net, Tokyo, Japan) was applied to the sperm culture. After vigorous mixing and further incubation at room temperature for 10 min, the chemiluminescent signal was measured using a Luminescencer JNRII plate reader (Atto, Tokyo, Japan).

Intracellular glucose and lactate assays

Frozen–thawed sperm (~ 5×10^6 sperm per mouse) were incubated in 50 µL of HTF medium for 30 min. The sperm (25,000 per each sample) were then resuspended in 0.1% Triton X-100 containing 0.3 mL of water and centrifuged at 15,000×*g* for 10 min at 4 °C. Intracellular glucose and lactate content were determined from the resulting supernatant, using glucose and lactate assay kits (Dojindo, Kumamoto, Japan). Absorbance at 450 nm was measured using a VICTOR Nivo multimode microplate reader (Perkin Elmer, Waltham, MA, USA).

FACS analysis of sperm

To detect mitochondrial membrane potential, the sperm (1×10^5 sperm per mouse) were stained with tetramethylrhodamine methyl ester (TMRM; 20 nM; Setaresh Biotech, Eugene, OR, USA). The intracellular pH and calcium ion levels of the sperm were evaluated using the respective chemical probes, BCECM-AM (3 µM; Dojindo) and Calbryte-520AM (10 µg/mL; AAT Bioquest, Sunnyvale, CA, USA). After pre-culture in HTF medium at 37 °C for 30 min, the sperm were stained with one of the aforementioned dyes at 37 °C for 15 min. After excluding the dead sperm with 7-amino-actinomycin D staining (Biolegend), the fluorescence signals of ~ 25,000 live sperm were monitored using FACSVerse (BD Biosciences).

In vitro fertilization (IVF)

Ova were isolated from adult female C57BL/6 mice (SLC) that were pre-treated with 7.5U pregnant mare serum gonadotropin (Asuka Animal Health, Tokyo, Japan) and 7.5U human chorionic gonadotropin (Asuka Animal Health). The sperm were introduced into the ~ 60 ovum suspension at 4×10^5 total live sperm/mL. After 4 h of incubation in HTF medium or PBS at 37 °C, the ova were transferred to a potassium simplex-optimized medium supplemented with 4 mg/mL BSA and further incubated for up to 1 day. The ova were observed using an IX71 microscope.

Immunocytochemistry and quantitative-fluorescent in situ hybridization (Q-FISH) analyses

The testis or epididymis was cut into small pieces and treated with collagenase (2 mg/mL, Sigma-Aldrich) and DNase I (4 U/mL, New England Biolab) in Tyrode solution at 37 °C for 20 min with vigorous mixing. The cell suspension was filtered with a cell strainer (BD Biosciences), applied to three

times the volume of NycoPrep 1.077 (Axis-Shield, Oslo, Denmark), and then centrifuged at 2500×*g* for 25 min. The interphase was collected and washed extensively with PBS. The cells (~50,000 per mouse) were resuspended in RPMI1640 medium supplemented with 10% FCS and then added to a well of a Biocoat fibronectin-coated high content imaging plate (Corning, Bedford, MA, USA). After incubation at 37 °C for 24 h, floating cells were removed by extensive washing with RPMI1640 medium. The remaining cells were subjected to immunocytochemistry and/or Q-FISH analyses.

For immunocytochemistry, the cells were fixed with 4% paraformaldehyde in PBS at room temperature for 10 min, and then treated with 0.3% Triton X in PBS for 15 min. The cells were then labeled with rabbit anti-mouse/human GM-CSF antibody (Abcam, 1/200-fold dilution) and biotinylated rat anti-mouse/human CD11b antibody (Biolegend, 1/200-fold dilution) at room temperature overnight. After washing with PBS, the immunocomplexes were visualized with Alexa Fluor 488-conjugated anti-rabbit antibody (Abcam, 1/1,000-fold dilution) and Alexa Fluor 555-conjugated streptavidin (Thermo Fisher Scientific, 1/1,000-fold dilution) at room temperature for 1 h. Fluorescent images were captured using a Nikon C2 laser confocal microscope and analyzed using ImageJ software [47].

Q-FISH analysis was performed using the ViewRNA Cell assay kit (Thermo Fisher Scientific), using synthetic probes for *Csf2* (Thermo Fisher Scientific). After the Q-FISH reaction, the sections were further subjected to immunofluorescent staining as described above, with anti-CD11b antibodies. To quantify *Csf2* expression, the number of $CD11b^+$ cells was counted in > 10 microscope fields of 60× magnification per sample. Then, the number of dots representing *Csf2* mRNA was counted, and the ratios of *Csf2* mRNA signals per $CD11b^+$ cells were calculated. More than 100 $CD11b^+$ cells per mouse were analyzed.

Statistical analysis

Data were analyzed using either Student's *t* test or one-way analysis of variance, followed by Tukey's test, in the KaleidaGraph software package (Hulinks, Tokyo, Japan).

Results

Myeloid-selective *Usp2* knockout does not vitally affect macrophage subpopulations in the testis

To evaluate whether the myeloid-selective *LyzM* promoter selectively drives macrophages of the testis, we crossed *LyzM-Cre* mice with R26GRR reporter mice. Cells from the myeloid lineage in the R26GRR/*LyzM-Cre* mice exhibited red fluorescence, while all other cells had green fluorescence (Supplementary Fig. 1a). Red fluorescent signals were observed in macrophage-like cells in the spleen, lung, jejunum, mesenteric lymph node, and liver (Supplementary Fig. 1b, c). In the testis, red fluorescent cells were observed in the interstitial and peritubular regions, where macrophages are known to be localized (Supplementary Fig. 1d). Most red fluorescent cells expressed the mouse macrophage marker F4/80, and red fluorescent signals were absent in other cell types, including Leydig cells, Sertoli cells, and the male germinative cell lineage. Similar findings were obtained in the epididymis; red fluorescence co-localized in $F4/80^+$ myeloid cells, which extruded processes from the peritubular region to the apical region (Supplementary Fig. 1e). After establishing that the *LyzM* promoter is exclusively activated in testicular macrophages, we next obtained myeloid-selective *Usp2*KO (ms*Usp2*KO) mice by crossing *LyzM-Cre* mice with $Usp2^{fl/fl}$ mice, and then crossing the $Usp2^{fl/+}$/*LyzM-Cre* offspring with $Usp2^{fl/fl}$ mice (Fig. 1a). *Cre* was selectively expressed in the testis and the peritoneal macrophages in ms*Usp2*KO mice, but not $Usp2^{fl/fl}$ mice (Supplementary Fig. 2a). Genomic PCR confirmed that the deletion of exons 3 and 4 of the *Usp2* gene occurred in the testis and in peritoneal macrophages of ms*Usp2*KO mice, but not in $Usp2^{fl/fl}$ mice (Supplementary Fig. 2b).

Since macrophages can be classified by surface marker patterns, we characterized the testicular macrophages derived from ms*Usp2*KO mice. As shown in Fig. 1b, the proportion of $F4/80^+$, $CD11b^+$ macrophages in ms*Usp2*KO mice was almost identical to that in $Usp2^{fl/fl}$ mice (Fig. 1b). Similarly, the proportion of $F4/80^+$, $CD11b^+$ macrophages was not modified in the spleen of ms*Usp2*KO mice (Supplementary Fig. 3a). On the other hand, $F4/80^+$, $CD11b^+$ macrophages were slightly increased in the peritoneal cavity of ms*Usp2*KO mice (Supplementary Fig. 3b). *Usp2* deficiency did not substantially affect localization of $F4/80^+$ macrophages in the spleen, liver, mesenteric lymph nodes, and intestine (Supplementary Fig. 4a–d).

Since the immunosuppressive M2 macrophage population is dominant in the testis [7], we examined the M1/M2 subclassification of the macrophages using FACS. In the testis of $Usp2^{fl/fl}$ mice, a large population of $F4/80^+$, $CD11b^+$ cells were $Ly6c^{int}$, $CD206^+$ M2-like macrophages (Fig. 1c). A similar proportion of $Ly6c^{int}$, $CD206^+$ cells were also observed in ms*Usp2*KO mice. On the other hand, the proportion of $Ly6c^{high}$, $CD206^-$ M1-like macrophages in the population of $F4/80^+$, $CD11b^+$ cells was remarkably low (~0.6%) in both $Usp2^{fl/fl}$ mice and ms*Usp2*KO mice, although this proportion was slightly smaller in ms*Usp2*KO mice than in $Usp2^{fl/fl}$ mice. Therefore, *Usp2* deficiency does not practically affect the dominance of M2 macrophages in the testis. Additionally, the ratio of M1 to M2 macrophages was not influenced by macrophage-selective *Usp2* deficiency

in the spleen and peritoneal cavity (Supplementary Fig. 3c, d). Thus, USP2 does not determine the direction of M1 and M2 predominance in the tissues, including the testis.

Because testicular macrophages can be classified into two subpopulations based on localization [9], we measured the proportion of interstitial and peritubular macrophages. Histological analysis demonstrated that interstitial and peritubular macrophages could be observed in both ms*Usp2*KO mice and *Usp2*$^{fl/fl}$ mice (Fig. 1d). The presence of interstitial and peritubular macrophages in the testis of both strains was further confirmed with the detection of CSF1R^{+} cells and MHCII^{+} cells in the respective areas (Supplementary Fig. 5). A similar proportion of interstitial CSF1R^{+} MHCII^{-} and peritubular CSF1R^{-} MHCII^{+} macrophages were observed in the ms*Usp2*KO mice and *Usp2*$^{fl/fl}$ mice (Fig. 1e). Thus, *Usp2* deficiency does not affect the testicular macrophage subpopulations.

Testicular macrophage USP2 does not affect the structure of the testis

Because testicular macrophages are crucial for the organogenesis of testis [12], we assessed the effect of macrophage *Usp2*KO on testicular morphology. As shown in Fig. 2a, b, the size and weight of the testis were hardly distinguishable between ms*Usp2*KO mice and *Usp2*$^{fl/fl}$ mice. Additionally, ms*Usp2*KO mice did not show alterations in the outer diameter and wall thickness of seminiferous tubes, both of which are indices for spermatogenesis (Fig. 2c). We further assessed the number and localization of several testicular cells using immunohistochemical techniques. An intense Ki67 immunological signal was evident in the spermatogonia and primary spermatocytes of *Usp2*$^{fl/fl}$ mice (Fig. 2d and Supplementary Fig. 6). A similar staining pattern of Ki67 was also observed in ms*Usp2*KO mice. Moreover, ms*Usp2*KO mice did not show any morphological changes in DEAD-box helicase (DDX) 4-positive spermatocytes compared to *Usp2*$^{fl/fl}$ mice (Fig. 2e and Supplementary Fig. 6). Similarly, monocarboxylate transporter (MCT) 1-positive Leydig cells and sex-determining region Y-box transcription factor (Sox) 9-positive Sertoli cells showed a principally similar staining pattern in ms*Usp2*KO mice and *Usp2*$^{fl/fl}$ mice (Figs. 2f, g and Supplementary Fig. 6). Taken together, macrophage USP2 has been shown to be dispensable for spermatogenesis and testicular organogenesis.

Testicular macrophage USP2 does not modulate testosterone and retinoic acid synthesis

Although ms*Usp2*KO mice did not manifest changes in the number of Leydig cells (Fig. 2f), *Usp2* ablation in testicular macrophages might affect testosterone signal. In mice, 3-β-hydroxysteroid dehydrogenase (HSD3B) 1 and 6 are key enzymes of testosterone production. As shown in Supplementary Fig. 7a-(i), the gene expression of *Hsd3b1*and *Hsd3b6* was not influenced in ms*Usp2*KO mice. Accordingly, blood and testicular testosterone levels were negligibly affected in ms*Usp2*KO mice (Supplementary Fig. 7b). Moreover, ms*Usp2*KO mice did not manifest changes in the expression of the luteinizing hormone receptor (*Lhcgr*) and androgen receptor (*Ar*), which were a releasing stimulant and a testosterone receptor in the testis, respectively [Supplementary Fig. 7a-(ii)].

Numerous studies have shown that retinoic acid, which has been postulated to be produced in testicular macrophages [9], plays a crucial role in spermatogenesis [48]. Thus, we measured the level of *Aldh1a2* and *Rdh10* expression, both of which encode enzymes involved in retinoic acid synthesis. As shown in Supplementary Fig. 7a-(iii), no changes in *Aldh1a1* or *Rdh10* expression were observed in the testis of ms*Usp2*KO mice. There were also no differences in the level of retinoic acid 8 (*Stra8*) expression, a typical retinoic acid-responsive gene [49], in the testis between ms*Usp2*KO mice and *Usp2*$^{fl/fl}$ mice [Supplementary Fig. 7a-(iv)]. Taken together, macrophage USP2 does not have a significant impact on testosterone or retinoic acid synthesis in the testis.

Testicular macrophage USP2 did not affect the morphology, viability, motility, and capacitation of freshly isolated sperm

We next studied the characteristics of mature sperm in ms*Usp2*KO mice. As shown in Fig. 3a, b, the morphology of sperm in the testis and epididymis was not different between ms*Usp2*KO mice and *Usp2*$^{fl/fl}$ mice. Moreover, the density of the epididymal sperm in ms*Usp2*KO mice was almost identical to that of *Usp2*$^{fl/fl}$ mice (Fig. 3c). Similarly, sperm viability was barely modified in ms*Usp2*KO mice (Fig. 3d). Thus, macrophage USP2 was not a prerequisite for the generation, viability, and morphogenesis of sperm.

A previous study demonstrated that *Usp2*KO mice exhibited decreased sperm motility [37]. We therefore assessed sperm motility in ms*Usp2*KO mice and *Usp2*$^{fl/fl}$ mice, and found no differences in the proportion of total motile sperm in ms*Usp2*KO mice compared to *Usp2*$^{fl/fl}$ mice (Fig. 3e). Moreover, progressive motility, which is characterized by markedly fast rectilinear motility and hyperactive curvilinear motility, was observed in the ms*Usp2*KO mice (Fig. 3f). After sperm preincubation in PBS instead of HTF medium, macrophage-selective *Usp2* deficiency did not influence total and progressive motility of sperm (data not shown). We further performed CTC staining to examine the rate of sperm capacitation. Capacitated sperm showed scarce staining in the postacrosomal area (Fig. 3g). We found that capacitation in ms*Usp2*KO mouse sperm was comparable to that of *Usp2*$^{fl/fl}$ mouse sperm. Collectively, macrophage USP2

does not influence the morphology, viability, motility, and hyperactivation of freshly isolated sperm.

Testicular macrophage USP2 promotes motility, hyperactivation, and capacitation of frozen–thawed sperm

Frozen–thawed sperm is widely applied in the treatment of infertility, generation of livestock animals, and conservation management of endangered species [50–52]. To investigate whether macrophage USP2 modifies sperm cryopreservation, we compared several characteristics of the frozen–thawed sperm from ms*Usp2*KO mice and *Usp2*$^{fl/fl}$ mice. As with freshly isolated sperm, the morphology of the frozen–thawed sperm was indistinguishable between the strains (Fig. 4a). The freezing and thawing evenly promoted cell death from 91 to 49% and from 96 to 42% in ms*Usp2*KO mice and *Usp2*$^{fl/fl}$ mice, respectively (Figs. 3d, 4b). Thus, macrophage USP2 is dispensable in maintaining morphology and viability during manipulation with freezing and thawing. In marked contrast, the proportion of total motile sperms was decreased by approximately one-fourth in ms*Usp2*KO mice compared to *Usp2*$^{fl/fl}$ mice (Fig. 4c). Furthermore, progressive motile sperm were more severely decreased in ms*Usp2*KO mice (Fig. 4c). Similarly, ms*Usp2*KO mouse-derived sperm showed significant defects in VSL, VCL, and amplitude of lateral head displacement (ALH), whereas beat-cross frequency (BCF) tended to be attenuated ($P = 0.053$, $n = 6$). Thus, macrophage USP2 could maintain motility of frozen–thawed sperm.

We also analyzed CASA data, using the K-means clustering method, to evaluate the proportion of hyperactive motile sperm [45]. As shown in Supplementary Fig. 8, the frozen–thawed sperm could be classified into four clusters based on VSL and VCL. Sperm belonging to Cluster #2 exhibited progressive curvilinear motion, which indicated hyperactivation. The proportion of hyperactive sperm was ~ 79% lower in ms*Usp2*KO mice than in *Usp2*$^{fl/fl}$ mice (Fig. 4d), suggesting that macrophage USP2 preserves the capacity for hyperactivation after exposure to the freeze–thaw process.

We next examined the effects of macrophage *Usp2* deficiency on capacitation rate in the frozen–thawed sperm. Approximately, 8.5% of frozen–thawed sperm from *Usp2*$^{fl/fl}$ mice were capacitated in HTF medium after incubation for 30 min (Fig. 4e). On the other hand, capacitation occurred in only ~ 4.8% of ms*Usp2*KO mouse sperm. Taken together, our results show that macrophage USP2 potentiates motility, hyperactivation, and capacitation of frozen–thawed sperm.

We further investigated several biochemical and physiological indices that are associated with hyperactive motility and capacitation in sperm. Because sperm activation is highly dependent on ATP supply [20], we measured the intracellular ATP level of the frozen–thawed sperm. The ATP level of ms*Usp2*KO mouse-derived sperm was ~ 74% of the *Usp2*$^{fl/fl}$ mouse-derived sperm (Fig. 5a), indicating that macrophage *Usp2* deletion inhibits the ATP supply in sperm.

Because glycolysis is necessary for hyperactive sperm motility and capacitation, we measured glycolytic activity by quantifying intracellular lactate and glucose content in

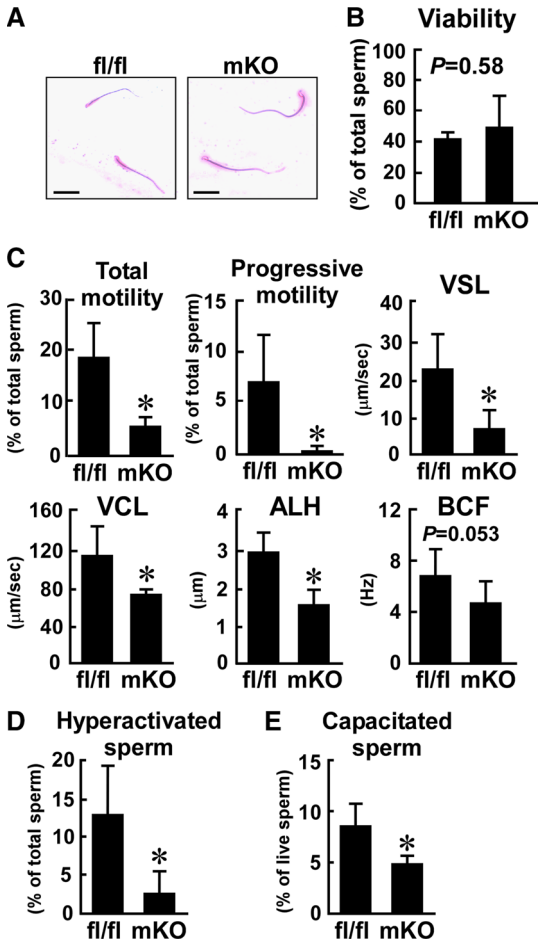

Fig. 4 Effect of myeloid-selective *Usp2* knockout on the motility, hyperactivation, and capacitation of frozen–thawed sperm. Sperm of myeloid-selective *Usp2* knockout mice (mKO) and *Usp2*$^{fl/fl}$ mice (fl/fl) were subjected to the freeze–thaw process. **a** The morphology of the epididymal sperm. Scale bars represent 50 μm. Representative microscopic images were obtained from five mice. **b** The viability of the epididymal sperm. **c** Sperm motility assessed by CASA. Total motility, progressive motility, straight-line velocity (VSL), curvilinear velocity (VCL), amplitude of lateral head displacement (ALH), and beat-cross frequency (BCF) of sperm were evaluated. **d** The proportion of hyperactivated sperm. K-means clustering was used to analyze the CASA data. Hyperactive sperm belonged to the cluster with high VCL and low linearity, as shown in Supplementary Fig. 8. **e** The proportion of capacitated sperm. Capacitation was determined by CTC staining. Approximately 200 (**b**, **e**), 300 (**c**), 340 (**d**, mKO), or 420 (**d**, fl/fl) sperm from each mouse was used for analysis. Data are shown as means ± SD of five (**b**, **e**) or six (**c**, **d**) mice. *$P < 0.05$ vs. *Usp2*$^{fl/fl}$ mice (**c**–**e**). The *P* values are also shown in the graphs (**b**, **c**)

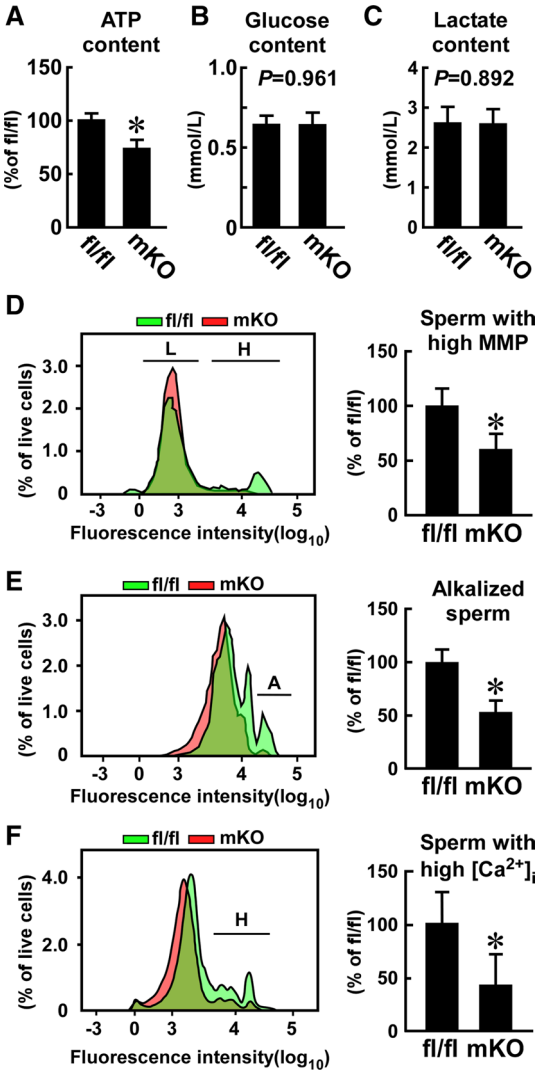

Fig. 5 Effect of myeloid-selective *Usp2* knockout on the biochemical and physiological responses of frozen–thawed sperm. **a**, **b**, **c** Intracellular ATP (**a**), glucose (**b**), and lactate (**c**) contents. Approximately 10,000 (**a**) or 25,000 (**b**, **c**) sperm per mouse was used for the analyses. **d**, **f** FACS analysis of mitochondrial membrane potential (MMP, **d**), intracellular pH (**e**), and calcium ion content (**f**) assessed with TMRM, BCECF-AM, and Calbryte-520AM, respectively. FACS images indicate sperm with high (H, **d**) and low (L, **d**) MMP, high alkalization (A, **e**), and high calcium influx (H, **f**) (left). The proportion of sperm with high MMP (**d**), high alkalization (**e**), and high calcium influx (**f**) in approximately 25,000 live sperm are also indicated (right panel). Data are shown as the means ± SD of six mice (**a–f**). *$P < 0.05$ vs. $Usp2^{fl/fl}$ mice. *P* values are also shown in graphs (**b**, **c**)

sperm. However, we found no differences in either intracellular lactate or glucose levels between sperm from $Usp2^{fl/fl}$ mice and sperm from ms*Usp2*KO mice (Fig. 5b, c), which indicate that macrophage USP2 is not vital for the maintenance of glycolysis in frozen–thawed sperm.

In contrast to hyperactive motility and capacitation, total sperm motility is highly associated with OXPHOS [20], whose activity can be evaluated by measuring mitochondrial membrane potential (MMP). Although both high- and low-MMP subpopulations were detected in the $Usp2^{fl/fl}$ mice, the high-MMP sperm population was smaller or negligible in the ms*Usp2*KO mice (Fig. 5d). Therefore, our results suggest that macrophage USP2 potentiates mitochondrial integrity, but not glycolysis, in a fraction of sperm, which contributed to greater ATP accumulation in the cells.

Sperm undergo alkalization upon the induction of capacitation, especially in the head and principal piece [53]. Alkalization in the principal piece has also been shown to initiate hyperactive motility [53]; therefore, we investigated whether macrophage USP2 influenced sperm alkalization by monitoring the intracellular pH using a pH-sensitive probe. After incubation in HTF medium for 30 min, $Usp2^{fl/fl}$ mouse-derived sperm comprised a dominant population with relatively low pH and a smaller alkalized population (17.2 ± 6.4%, $n = 5$, Fig. 5e). This proportion of alkalized sperm was significantly decreased in the ms*Usp2*KO mouse-derived sperm compared to $Usp2^{fl/fl}$ mouse-derived sperm. Therefore, macrophage USP2 sustains hyperactivation-associated alkalization in frozen–thawed sperm.

CatSper is a sperm-specific calcium channel that mediates high pH-evoked calcium influx, which triggers sperm hyperactivation [22, 23]. We therefore investigated the intracellular calcium levels in sperm using a calcium probe (Fig. 5f). FACS analysis revealed relatively low fluorescence in 89.2% of live sperm from $Usp2^{fl/fl}$ mice, while a > tenfold signal was observed in the remaining 10.8% of sperm, indicating that ~ 11% of total sperm from $Usp2^{fl/fl}$ mice displayed an extreme calcium influx. In contrast, only 2.2% of sperm from ms*Usp2*KO mice showed a similar degree of calcium influx. Therefore, the results suggest that macrophage USP2 potentiates calcium influx in frozen–thawed sperm, which may elicit sperm hyperactivation.

Because inhibition of alkalization and intracellular calcium ion accumulation were observed in the sperm from ms*Usp2*KO mice, we used qRT-PCR to measure the mRNA expression levels of canonical ion channels and pumps in the testis. Macrophage *Usp2* deficiency did not modify the expression of the spermatic channels and pumps that participate in alkalization, such as voltage-gated hydrogen channel 1 (*Hvnc1*) and solute carrier family 9 member C1 (*Slc9c1*) (Supplementary Fig. 9). Similarly, the expression of CatSper subunits was negligibly affected in the sperm of ms*Usp2*KO mice. Therefore, macrophage USP2 controls sperm hyperactivation independently of changes in the expression of the spermatic channels and pumps that we examined.

Testicular macrophage USP2 increases the in vitro fertilizing capacity of frozen–thawed sperm

Decreased motility, capacitation, and hyperactivation of the frozen–thawed sperm from ms*Usp2*KO mice might affect fertility. To examine this, we performed IVF using frozen–thawed sperm from ms*Usp2*KO mice and *Usp2*$^{fl/fl}$ mice. The sperm of both strains evenly induced dispersion of the cumulus (Fig. 6a). Subsequently, ~ 40,000 sperm from *Usp2*$^{fl/fl}$ mice caused at least one polar body in 55.4 ± 16.8% of ova from C57BL/6 mice after 4 h of incubation (Fig. 6b, c). Almost the same number of sperm from ms*Usp2*KO mice formed polar bodies, at a comparable proportion (51.5 ± 17.1%, $P = 0.674$ vs *Usp2*$^{fl/fl}$ mice, $n = 7$). On the other hand, the formation of pronuclei was dramatically repressed in the ova that were incubated with sperm from ms*Usp2*KO mice, compared to those of *Usp2*$^{fl/fl}$ mice (ms*Usp2*KO mice, 5.93 ± 6.8%; *Usp2*$^{fl/fl}$ mice, 20.8 ± 13.8%: $P = 0.025$, $n = 7$: Fig. 6b, d). Therefore, frozen–thawed sperms from ms*Usp2*KO mice had lower IVF efficiency.

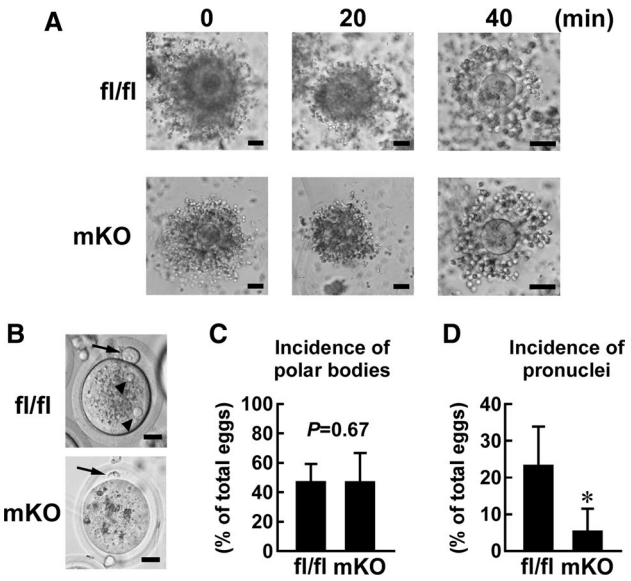

Fig. 6 Effect of myeloid-selective *Usp2* knockout on the efficiency of in vitro fertilization. Frozen–thawed 4×10^4 live sperm, which were isolated from myeloid-selective *Usp2* knockout mice (mKO) and *Usp2*$^{fl/fl}$ mice (fl/fl), were subjected to in vitro fertilization (IVF) using the ova of C57BL/6 mice. Approximately, 60 ova were used for an IVF series. **a** Dispersion of cumulus cells. Ova surrounded with cumulus cells were incubated with sperm from the mice for 0, 20, and 40 min. **b** Ova after 8 h incubation with sperm. Arrows and arrowheads represent polar bodies and pronuclei, respectively. **c**, **d** Incidence of polar bodies (**c**) or pronuclei (**d**) in ova after incubation with sperm. Representative images of seven IVF series are shown (**a**, **b**). Scale bars represent 50 (**a**), or 20 (**b**) µm. Data are shown as means ± SD of seven male mice (**c**, **d**). *$P < 0.05$ vs *Usp2*$^{fl/fl}$ mice (**d**). *P* value is also shown (**c**)

USP2 sustains GM-CSF expression in testicular interstitial macrophages

Cumulative evidence indicates that USP2 regulates inflammatory cytokine production in macrophages [29, 33–35]. Since several cytokines modify sperm motility [54], we compared the expression of 43 cytokine genes as well as that of *Serpine1* and *Serpine2* in the testis of ms*Usp2*KO mice and *Usp2*$^{fl/fl}$ mice. qRT-PCR analysis demonstrated that the expression levels of inflammatory cytokines such as *Il1b*, *Il6* and *Tnf* were not distinguishable between the strains (Fig. 7a). Similarly, most cytokines which we examined did not show significant changes in the testis after *Usp2* ablation (Fig. 7a). Conversely, transcripts for *Csf2* (encoding GM-CSF) were significantly (0.46-fold, $P = 0.0028$, $n = 6$) decreased in the testis of ms*Usp2*KO mice compared with *Usp2*$^{fl/fl}$ mice (Fig. 7a, b). Moreover, *Serpine 1* was slightly, but significantly (0.79-fold, $P = 0.0090$, $n = 6$) downregulated in the testis of ms*Usp2*KO mice (Fig. 7a). Therefore, macrophage USP2 may have some influence overexpression of *Csf2* and *Serpine 1* in testis. Because *Csf2* is known to potentiate total motility and hyperactive motility of frozen–thawed ovine sperm [19], we further investigated the roles of GM-CSF in macrophage USP2-mediated sperm regulation.

To verify the sources of GM-CSF in the testis, we performed an immunofluorescent analysis using C57BL/6 mouse testis. An immunoreactive signal for GM-CSF was especially apparent in some parts of F4/80$^+$ cells in the interstitial region (Fig. 7c), and this signal disappeared when the anti-GM-CSF antibody was pre-incubated with an excess amount of recombinant GM-CSF (Supplementary Fig. 10a). Therefore, interstitial macrophages appear to produce GM-CSF in the testis. In further agreement with our data, immunoreactivity against GM-CSF was also observed in isolated CD11b$^+$ testicular macrophages (Fig. 7d). Incubation with pre-adsorbed anti-GM-CSF antibody, or the secondary antibody without the anti-CD11b antibody, did not generate any signal (Supplementary Fig. 10b, c), leading us to conclude that the immunoreactive signals for GM-CSF and CD11b were specific. Furthermore, Q-FISH analysis detected signals corresponding to *Csf2* mRNA in certain populations of C57BL/6 mouse-derived testicular macrophages, which were not observed without the *Csf2* probe (Supplementary Fig. 10d). qRT-PCR analysis (Fig. 7a) further detailed that the mean number of *Csf2* fluorescent dots was decreased by ~ 37% in ms*Usp2*KO mouse-derived testicular macrophages, compared to those of *Usp2*$^{fl/fl}$ mice (Fig. 7e, f). Collectively, our data suggest that testicular macrophages have the potential to produce GM-CSF, and that *Usp2* potentiates *Csf2* expression in testicular macrophages.

Sperm undergo posttesticular maturation in the epididymis, in preparation for capacitation in the female

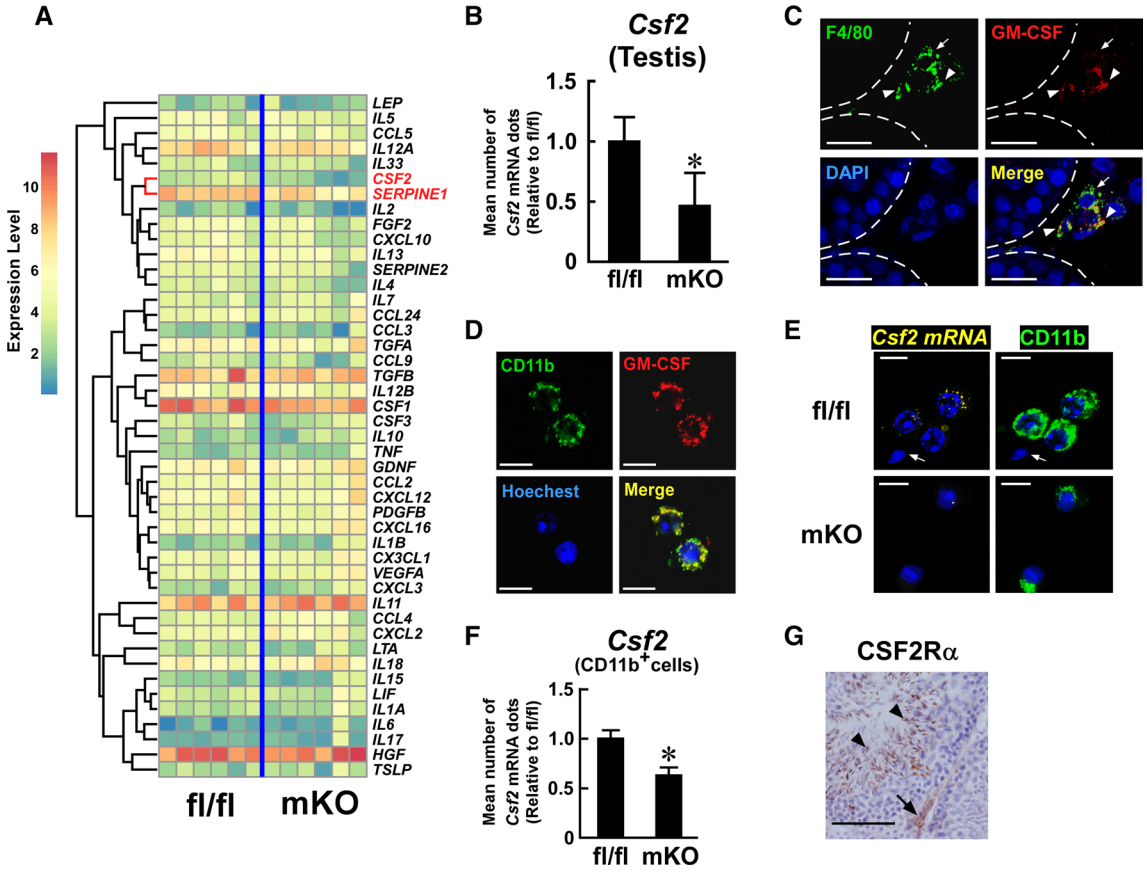

Fig. 7 Effect of myeloid-selective *Usp2* knockout on *Csf2* expression in the testis. **a** Comprehensive qRT-PCR for cytokine expression in the testis of myeloid-selective *Usp2* knockout mice (mKO) and $Usp2^{fl/fl}$ mice (fl/fl). The clustering tree is drawn on the left of the heatmap. The *Csf2* and *Serpine 1* rows are highlighted. **b** qRT-PCR analysis of *Csf2* expression in the testis. Data were normalized to the level of *Hprt1* expression. **c**, **d** Immunofluorescent detection of GM-CSF (red) and F4/80 (green, **c**) or CD11b (green, **d**) in the testis (**c**) or isolated testicular adherent cells (**d**) of C57BL/6 mice. Dashed lines show seminiferous tubules (**c**). Arrows and arrowheads indicate GM-CSF$^-$, F4/80$^+$ and GM-CSF$^+$, F4/80$^+$ cells, respectively (**c**). **e**, **f** Q-FISH analysis of *Csf2* expression in the testicular adherent fraction of myeloid-selective *Usp2* knockout mice (mKO) and $Usp2^{fl/fl}$ mice (fl/fl). Representative images for Q-FISH for *Csf2* mRNA (**e**) and the mean abundance of *Csf2* mRNA dots in CD11b$^+$ cells (**f**) are shown. An arrow indicates sperm (**e**). The number of *Csf2* mRNA dots were counted in 100 randomly selected CD11b$^+$ cells in 10 microscopic fields for each mouse (**f**). **g** Representative images of CSF2 receptor α chain (CSF2R α)-immunostaining in the testis of C57BL/6 mice. An arrow and arrowheads indicate a CSF2R α$^+$ spermatid and testicular interstitial cells, respectively. Nuclei were stained with DAPI (**c**), Hoechst33342 (**d**, **e**), and hematoxylin (**g**). Scale bars represent 20 μm (**c**, **g**) and 15 μm (**d**, **e**). Data are shown as means ± SD of six (**b**) or five (**f**) mice. Microscope analyses were reproducibly obtained from three (**c**, **g**), four (**d**), or seven (**e**) mice. $*P < 0.05$ vs $Usp2^{fl/fl}$ mice (**b**, **f**)

reproductive tract [55]. In the epididymis, myeloid cells extrude projections to the adluminal site of the epididymal duct [56–58]. Thus, macrophages in the epididymis may contribute to priming sperm for hyperactivation and capacitation. To clarify whether USP2 modulates GM-CSF production in epididymal macrophages, we first evaluated the expression of GM-CSF in the epididymis. Immunoreactive signals for GM-CSF was apparent in the supranuclear region of principal epithelial cells [Supplementary Fig. 11a, b-(i)] and in intraluminal clear epithelial cells [Supplementary Fig. 11a, b-(ii)] in the corpus of the epididymis of C57BL/6 mice, corroborating a recent report on boar epididymis [59]. In addition, intense GM-CSF signals were detected in vesicles in the lumen [Supplementary Fig. 11a, b-(iii)]. GM-CSF was also present in peritubular cells with slender dendrites extending toward the luminal region [Supplementary Fig. 11a, b-(iv)]. GM-CSF$^+$ peritubular cells were also F4/80-positive, suggesting that epididymal macrophages produce GM-CSF (Supplementary Fig. 11c). To confirm GM-CSF expression in epididymal macrophages, we examined GM-CSF immunoreactivity in isolated epididymal CD11b$^+$ macrophages. As observed in the testis, GM-CSF immunoreactive signals were observed in CD11b$^+$ cells, which were dampened when incubated with anti-GM-CSF antibody that was pre-adsorbed with recombinant GM-CSF (data not shown). Together, these results indicate that macrophages are a source of GM-CSF in the epididymis, but the degree of their contribution is still unclear.

We next investigated the role of macrophage USP2 in *Csf2* expression in the epididymis. Compared to *Usp2*$^{fl/fl}$ mice, the level of epididymal *Csf2* mRNA was 32% lower in ms*Usp2*KO mice (Supplementary Fig. 11d). Furthermore, Q-FISH analysis demonstrated that the mean number of *Csf2* mRNA dots in CD11b^{+} cells were significantly decreased in ms*Usp2*KO mouse-derived epididymal macrophages than that of *Usp2*$^{fl/fl}$-derived macrophages (Supplementary Fig. 11e, 11f). Therefore, USP2 potentiates *Csf2* expression in epididymal macrophages.

We also investigated the expression of the GM-CSF receptor in testicular cells, and found that C57BL/6 mice expressed the CSF2 receptor α chain (CSF2R α) in both sperm and testicular interstitial cells (Fig. 7g). Taken together with previous papers [19], our results indicate that sperm are responsive to GM-CSF from testicular macrophages and/or epididymal cells.

GM-CSF restored macrophage *Usp2* knockout-elicited aberrant mitochondrial membrane potential and total sperm motility

GM-CSF promotes the cryoprotection of sperm resulting in the restoration of total sperm motility [19]. We thus assessed whether GM-CSF could overcome the aberrant total motility of the frozen–thawed sperm from ms*Usp2*KO mice. During the freezing and thawing process, the sperm from ms*Usp2*KO mice and *Usp2*$^{fl/fl}$ mice were treated with GM-CSF. After thawing, the GM-CSF pre-treatment elevated the total sperm motility of ms*Usp2*KO mice, while it marginally potentiated that of *Usp2*$^{fl/f}$ mice (Fig. 8a). As a result, the difference in total sperm motility between the strains was diminished by GM-CSF treatment.

Since total sperm motility is dominantly regulated by OXPHOS [20], we next examined whether GM-CSF recovered the mitochondrial membrane functionality of the frozen–thawed sperm. As shown in Fig. 8b, GM-CSF negligibly modulated the fraction of the sperm population in *Usp2*$^{fl/fl}$ mice with high MPP. In contrast, GM-CSF increased the number of sperm with high MPP in ms*Usp2*KO mice (Fig. 8b). Similarly, GM-CSF treatment restored the aberrant accumulation of ATP in the ms*Usp2*KO mouse sperm (Fig. 8c). Collectively, these experiments showed that the lack of GM-CSF might be attributed to defects in total motility and malfunction of mitochondrial activity in ms*Usp2*KO mouse sperm.

GM-CSF failed to restore progressive motility, capacitation, hyperactivation, and in vitro fertilization efficacy of the sperm from macrophage-selective *Usp2* knockout mice

We next assessed the effect of GM-CSF on progressive sperm motility in ms*Usp2*KO mice and *Usp2*$^{fl/fl}$ mice. As shown in Fig. 8d, GM-CSF increased the number of progressively motile sperm in *Usp2*$^{fl/fl}$ mice, whereas the increase in progressively motile ms*Usp2*KO sperm was marginal. Thus, GM-CSF did not significantly influence macrophage USP2-sustained progressive sperm motility.

The proportion of hyperactive sperm in progressive motile sperm is higher than that of total motile sperm. Because GM-CSF failed to restore progressive motility, but not total motility (Fig. 8a, d), GM-CSF might not contribute to sperm hyperactivation. To this end, we investigated the effect of GM-CSF on the size of the cluster that encompasses hyperactive sperm (Supplementary Fig. 12). GM-CSF did not mitigate a decrement of hyperactive sperm in ms*Usp2*KO mice (Fig. 8e) and failed to rescue the defective capacitation in ms*Usp2*KO sperm. In contrast, GM-CSF tended to promote capacitation in *Usp2*$^{fl/fl}$ sperm (Fig. 8f). Therefore, GM-CSF is not responsible for macrophage USP2-dependent hyperactivation or capacitation of frozen–thawed sperm.

Since alkalization is vital for hyperactivation and capacitation of sperm [20], we examined whether GM-CSF could modify the intracellular pH level of ms*Usp2*KO mouse sperm. FACS analysis of BCECM-AM-loaded sperm showed that GM-CSF did not affect the pH level of sperm from both ms*Usp2*KO mice and *Usp2*$^{fl/fl}$ mice (Fig. 8g). Furthermore, the proportion of alkalized sperm was significantly smaller in ms*Usp2*KO mice than in *Usp2*$^{fl/fl}$ mice, regardless of GM-CSF treatment (Fig. 8g). Similarly, GM-CSF did not alter the calcium influx in both ms*Usp2*KO mice and *Usp2*$^{fl/fl}$ mice (Fig. 8h). Therefore, the difference in intracellular calcium content was still evident between the strains after GM-CSF treatment.

Finally, we investigated the effect of GM-CSF on the IVF efficacy of ms*Usp2*KO sperm. As shown in Fig. 8i and Supplementary Fig. 13, GM-CSF did not rectify ova generation when incubated with ms*Usp2*KO sperm, but tended to increase the number of pronuclei in ova when incubated with *Usp2*$^{fl/fl}$ sperm. These results indicate that GM-CSF was unable to restore macrophage USP2-potentiated hyperactivation, capacitation, and IVF efficacy of sperm.

Discussion

Testicular macrophages are indisputably important in maintaining testicular function. For instance, elimination of testicular macrophages by liposome-entrapped dichloromethylene diphosphonate affected the proliferation and differentiation of Leydig cells during prepubertal development [14] and decreased testosterone synthesis by Leydig cells [13]. Additionally, both types of testicular macrophages significantly express enzymes for the biosynthesis of retinoic acid, which is crucial for spermatogenesis [9].

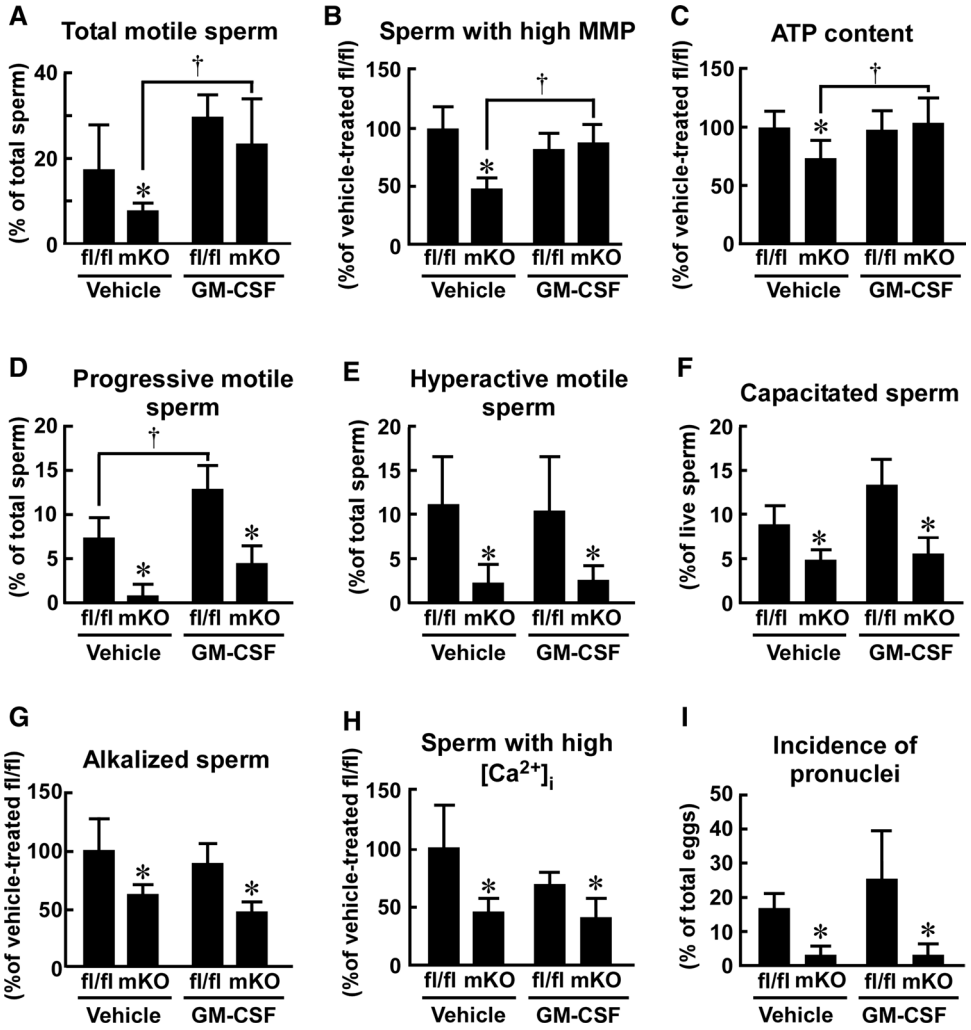

Fig. 8 Effect of GM-CSF on frozen–thawed sperm isolated from myeloid-selective *Usp2* knockout mice. Sperm from myeloid-selective *Usp2* knockout mice (mKO) and $Usp2^{fl/fl}$ mice (fl/fl) were treated with.either GM-CSF (5 nM) or vehicle, before and during the freeze–thaw process. **a** The proportion of total motile sperm. **b** The proportion of sperm with a high mitochondrial membrane potential (MMP). **c** The intracellular ATP content in total sperm. **d–f** The proportion of progressive motile sperm (**d**), hyperactive motile sperm (**e**), or capacitated sperm (**f**). **g**, **h** The proportion of sperm with high alkalization (**g**) and high intracellular calcium (**h**). **i** The incidence of pronuclei in eggs after in vitro fertilization. For each experiment, the presence of pronuclei in ~ 60 ova was evaluated after an 8 h incubation with sperm (4×10^5 sperm/mL). Approximately, 300 (**a**, **d**), 10,000 (**c**) 630 (**e**, mKO) or 460 (**e**, fl/fl) total sperm, or 25,000 (**b**, **g**, **h**) or 200 (**f**) live sperm from each mouse were used in these assays. Data are shown as the means ± SD of four (**d**, **f**), five (**a**, **b**, **g**, **h**, **i**), or six (**c**, **e**) mice. $^*P < 0.05$ vs $Usp2^{fl/fl}$ mice. $^\dagger P < 0.05$ vs. vehicle-treated groups (**a–d**)

The necessity of testicular macrophage presence in spermatogenesis was also proven by the observation that the depletion of macrophages led to a disruption in spermatogonia development [9] and to significant sperm reduction in seminal fluid [12]. In the present study, the morphological changes in spermatogonia as well as Leydig cells were not apparent in ms*Usp2*KO mice. Moreover, changes in testosterone levels were negligible in both the serum and testis. Therefore, macrophage USP2 seemed to be dispensable for spermatogenesis.

*Usp2*KO mice manifested male subfertility and abnormal aggregates consisting of sperm and multinucleated cells in seminiferous tubules [37]. Although the morphology of sperm in the epididymis was normal in *Usp2*KO mice, the sperm exhibited remarkable motility defects [37]. Because late-stage spermatids exclusively express USP2 [36], USP2 deficiency likely contributes to male subfertility in *Usp2*KO mice. The present study sheds new light on the roles of macrophage USP2 in sperm motility. Notably, the beneficial effects of macrophage USP2 are more prominent in frozen–thawed sperm than in freshly isolated sperm. Since frozen–thawed sperm are widely used in infertility treatments, genetic manipulation of livestock, and conservation management of endangered

animals, our study may provide important knowledge that is relevant to the medical and industrial fields [50–52].

Sperm motility can be classified into total and hyperactive motility [21]. Total motility is highly dependent on OXPHOS at the midpiece of sperm, while hyperactive motility dominantly utilizes ATP produced by glycolysis at the head and principal piece [20]. We demonstrated that macrophage USP2 maintained both total and hyperactive sperm motility. This observation implies that testicular macrophages modified both sperm motilities, regardless of the effects on morphological changes. Given that the total and hyperactive motilities are driven by distinct mechanisms, USP2 in testicular macrophages might function as a common regulator for both types.

Our current results demonstrated that macrophage-selective *Usp2* knockout did not cause significant changes in the expression of 19 canonical channels and pumps, all of which are postulated to have crucial roles in intracellular alkalization and calcium ion influx [21–23]. However, we were unable to exclude the possibility that macrophage USP2 modulates the expression of channels that were not examined in this study. Alternatively, macrophage USP2 may exert control over the expression of these membrane proteins at the post-transcriptional and/or translational level.

In IVF experiments, frozen–thawed sperm of ms*Usp2*KO mice caused normal polar body formation in the ova and dispersion of the ovarian cumulus. In sharp contrast, the sperm of ms*Usp2*KO mice had defects in the generation of ova pronuclei, indicating that ms*Usp2*KO mouse sperm lowered fertilization efficiency. Since hyperactive motility is believed to determine fertilization efficiency [21, 60], the inefficient IVF of ms*Usp2*KO mouse sperm is attributable to the decrease in hyperactive motile sperm. In the present study, macrophage-selective *Usp2* deficiency caused a reduction of the sperm population with high alkalization and high calcium influx. Given that alkalization-induced calcium influx confers hypermobility to sperm during capacitation [21, 23], macrophage USP2 might promote capacitation and hyperactivation of the frozen–thawed sperm, thereby leading to high IVF efficacy.

Previous evidence has indicated that testicular macrophage-derived cytokines modulate spermatogenesis [61]. Moreover, several cytokines also modify sperm functions, such as motility, chemotaxis, and the acrosome reaction [62–65]. In the present study, we found decreased *Csf2* expression in the testicular macrophages of ms*Usp2*KO mice. This observation is congruent with the results from a previous study that showed high levels of GM-CSF expression in testicular macrophages [18]. The finding that GM-CSF can access spermatogonial cells through the blood–testis barrier, which is formed by Sertoli cells and physically protects spermatogonial cells from systemic circulation [66], suggests that macrophage-derived GM-CSF can directly modulate the function of male gamete cells.

It has already been demonstrated that GM-CSF potentiates glucose uptake of sperm, possibly through the induction of glucose transporters [67], resulting in the promotion of motility of bovine sperm [68]. In our preliminary experiment, GM-CSF did not cause changes in the expression of glucose transporters in the sperm of ms*Usp2*KO mice and $Usp2^{fl/fl}$ mice. Nevertheless, application of GM-CSF during the freezing and thawing process reverted total sperm motility, mitochondrial membrane potential, as well as the intracellular ATP level. In this study, we did not uncover molecular mechanisms underlying GM-CSF promotion of mitochondrial integrity in sperm. Some heat shock proteins maintain mitochondrial membrane integrity [69, 70]. They are regulated by STAT3 [71], which GM-CSF activates [72]. Thus, macrophage USP2 might control mitochondrial integrity through the induction of chaperone proteins such as heat shock proteins by GM-CSF production.

In contrast to MMP and total sperm motility, GM-CSF failed to rescue defects in capacitation, hyperactivation, and subsequent IVF efficiency, all of which are predominantly fueled by glycolysis [20]. Our preliminary study showed that GM-CSF did not affect the intracellular content of glucose and lactate in either ms*Usp2*KO sperm or $Usp2^{fl/fl}$ sperm, indicating that glycolytic activity is not a prerequisite for USP2-modulated sperm activation. Capacitation and hyperactivation are initiated by changes in plasma membrane characteristics, including cholesterol efflux [22], which are reflected in the pattern of CTC staining [73]. Therefore, the impairment of changes in CTC staining that was observed ms*Usp2*KO sperm in this study suggests that macrophage USP2 maintains the initial stages of the capacitation process.

In addition to *Csf2*, we found that macrophage-specific *Usp2* deficiency led to a slight downregulation in *Serpine* 1 expression in the testis. The *Serpine 1* gene encodes plasminogen activator inhibitor (PAI-1), which inhibits plasminogen activators and encumbers plasmin production [74]. Because PAI-1 and plasminogen activator receptor bind to the sperm plasma membrane, the quantitative ratio of these counteracting proteins affects the proteolytic activity of the sperm membrane, as well as the modulation of capacitation efficiency [74]. Accordingly, the concentration of tissue-type plasminogen activator in spermatozoa has been shown to be higher in cases of human subfertility, which suggests that excessive activation of plasminogen activators contribute to sterility [75]. Therefore, although it is still unclear whether macrophage PAI-1 can reach sperm and/or spermatocytes through the blood–testis barrier, blunted PAI-1expression in testicular macrophages may participate in defective sperm hyperactivation in ms*Usp2*KO mice.

Compared to $Usp2^{fl/fl}$ sperm, total sperm motility in ms*Usp2*KO mice was decreased to 28.6% (Fig. 4c), whereas

ATP accumulation was only reduced by 25.4% (Fig. 5a). The presence of immotile sperm, which still contain ATP at a significant level [76], may account for the discrepancy between these indices. Thus, the reduction in ATP may in fact be relatively mild compared to the decrease in total sperm motility. Conversely, the mechanisms driving the differences between the changes observed in intracellular pH (~46.4% decrease, Fig. 5e) and that of progressive motility (~97.0% decrease, Fig. 4c) appear to be convoluted. After intracellular alkalization, several coordinated biochemical and physiological cellular events, such as calcium influx, protein kinase A activation, and tyrosine phosphorylation, occur during hyperactivation [21–23]. Therefore, macrophage USP2-mediated regulation of sperm function may involve multiple molecular targets.

In a previous study, we performed comprehensive qRT-PCR for cytokines and growth factors using *USP2* knockdown (KD) human macrophage-like HL-60 cells [29]. *USP2*KD HL-60 cells showed an increased expression of nine chemokines compared with parental HL-60 cells. Moreover, bacterial lipopolysaccharide provoked the expression of 25 of 104 cytokines in *USP2*KD HL-60 cells [34]. These results indicate that USP2 attenuated the induction of a relatively wide variety of proinflammatory cytokine genes. On the other hand, the testis of ms*Usp2*KO mice showed a decreased expression of only *Csf2* among 43 cytokines. This limited change in cytokine expression might be accounted for by technical issues. In the testis, the proportion of macrophages is limited, although they are the second most abundant cellular population after Leydig cells in the interstitial space [77]. Since a significant amount of cytokines is produced in other testicular cells [61, 78, 79], this might offset aberrant cytokine expression in macrophages. Alternatively, the differences in characteristics between HL-60 cells/peritoneal macrophages and testicular macrophages might yield differences in their USP2-modulated cytokine expression profiles. Differentiated HL-60 and peritoneal macrophages have the property of M1 macrophages, since their dominant population express CD11c, an M1 macrophage marker [29, 80, 81]. Since testicular macrophages contain an M2-dominant population [10], USP2 might have different effects on cytokine production between M1 and M2 macrophages.

In this study, we still did not evaluate molecular mechanisms underlying USP2-modulated *Csf2* expression. Although little is known about the mechanisms for *Csf2* induction in testicular macrophages, several signal cascades are believed to participate in *Csf2* induction in various type of cells [82, 83]. NF-κB is known to activate the *Csf2* promoter in various types of cells such as T-lymphocytes, macrophages and bladder carcinoma cells [83–85]. Previously, it has been shown that TNF-α-elicited NF-κB signaling is enhanced by USP2 [35]. On the other hand, we also showed that USP2 regulates the expression of various cytokines by modulating poly-ubiquitination of Oct 1 [34]. Further studies are required to identify USP2-targeting molecules that are responsible for *Csf2* expression in testicular macrophages. Such information might be helpful in understanding the molecular basis of communications between testicular macrophages and sperm.

Various types of myeloid cells, including macrophages and dendritic cells, exist in the interstitial and peritubular regions of the epididymis [58, 86]. The myeloid cells are postulated to maintain immune privilege in the epididymis; they play a role in pathogen defense and also maintain immune tolerance toward sperm antigens [58, 87]. In addition, epididymal myeloid cells eliminate apoptotic epithelial cells after unilateral efferent duct ligation [56], suggesting that they may also sustain epithelial integrity at a steady state, and can directly communicate with sperm via cell processes that project into the lumen of the epididymal duct [58, 87]. In this study, we observed GM-CSF expression in macrophages in epididymal sections and in isolated epididymal macrophages, which suggests that macrophages may regulate sperm function via GM-CSF secretion. In contrast to the testis, GM-CSF appears to be produced in various epididymal cell types, including principal and clear epithelial cells, both of which directly affect sperm on the luminal side. A previous report also demonstrated intense GM-CSF immunoreactivity in vesicles, which were suggested to have been released from principal epithelial cells [59]. Future study might clarify whether macrophage USP2 is involved in GM-CSF production in the epididymal epithelial cells via macrophage-to-epithelial communication.

To perform myeloid-selective *Usp2* knockout, we employed the *LyzM*-Cre cassette. The *LyzM*-Cre-dependent conditional knockout mouse strains have been widely used to evaluate in vivo roles of various molecules expressed in cells of myeloid lineage, including macrophages [88–90]. Another study demonstrated that the *LyzM* promoter is also active in neural brain cells [91]. Thus, we could not exclude the possibility that neural USP2 maintained the testicular function of ms*Usp2*KO mice through the hypothalamus–testis axis. However, our preliminary study indicated that neuron-selective *Usp2*KO mice yielded changes in neither *Csf2* expression nor sperm motility in testicular macrophages. We therefore conclude that macrophage USP2 is a positive regulator of *Csf2* expression and activation of frozen–thawed sperm.

Acknowledgements The authors would like to thank Dr. Keiji Ueno, Mr. Takeshi Ishino, Ms. Misato Amagasa, Ms. Aya Iida, and Ms. Marina Tanaka from Rakuno Gakuen University, and Dr. Yuko Okamatsu from Hokkaido University. The authors also acknowledge the editing services provided by Uni-edit.

Author contributions MH and SK performed the experiments, analyzed the data, and wrote and revised the manuscript. CK, YY, TW,

and ET performed the experiments. JO revised the manuscript. MN designed and performed the experiments and revised the manuscript. HK designed and performed the experiments, analyzed data, and wrote and revised the manuscript. All authors read and approved the final version of the manuscript.

Funding This work was supported by the Japan Society for the Promotion of Science KAKENHI (15K06805 and 18K06035) and the Rakuno Gakuen University Research Fund (No. 2018-02, 2019-03, and 2020-04).

Availability of data and material The datasets in this study are available from the corresponding author upon reasonable request.

Code availability All software used in this study was obtained legally, and custom code is available from the corresponding author on reasonable request.

Compliance with ethical standards

Conflict of interest The authors have no conflicts of interest/competing interests to declare.

Ethical approval All animal experiments were approved by the Ethical Review Committee for Animal Experimentation of Rakuno Gakuen University (Approval Numbers VH15A30, VH16A25, VH17A1). We made all efforts to reduce the number of animals used, and to alleviate their suffering.

Consent to participate/Consent for publication Consent to participate/consent for publication is not applicable to this study.

References

1. Kharraz Y, Guerra J, Mann CJ et al (2013) Macrophage plasticity and the role of inflammation in skeletal muscle repair. Mediat Inflamm 2013:491497. https://doi.org/10.1155/2013/491497
2. Lavine KJ, Pinto AR, Epelman S et al (2018) The Macrophage in cardiac homeostasis and disease: JACC macrophage in CVD series (part 4). J Am Coll Cardiol 72:2213–2230. https://doi.org/10.1016/j.jacc.2018.08.2149
3. Rosin JM, Kurrasch DM (2019) Emerging roles for hypothalamic microglia as regulators of physiological homeostasis. Front Neuroendocrinol 54:100748. https://doi.org/10.1016/j.yfrne.2019.100748
4. Benoit M, Desnues B, Mege J-L (2008) Macrophage polarization in bacterial infections. J Immunol 181:3733–3739. https://doi.org/10.4049/jimmunol.181.6.3733
5. Kitamura H, Naoe Y, Kimura S et al (2013) Beneficial effects of Brazilian propolis on type 2 diabetes in ob/ob mice. Adipocyte 2:227–236. https://doi.org/10.4161/adip.25608
6. Xiao-Ming M, Shiu-Kwong MT, Lan H-Y (2019) Macrophages in renal fibrosis. Adv Exp Med Biol 1165:285–303. https://doi.org/10.1007/978-981-13-8871-2_13
7. Meinhardt A, Wang M, Schulz C, Bhushan S (2018) Microenvironmental signals govern the cellular identity of testicular macrophages. J Leukoc Biol 104:757–766. https://doi.org/10.1002/JLB.3MR0318-086RR
8. Gaytan F, Bellido C, Morales C et al (1995) Response to Leydig cell apoptosis in the absence of testicular macrophages. J Reprod Immunol 29:81–94. https://doi.org/10.1016/0165-0378(95)00934-D
9. DeFalco T, Potter SJ, Williams AV et al (2015) Macrophages contribute to the spermatogonial niche in the adult testis. Cell Rep 12:1107–1119. https://doi.org/10.1016/j.celrep.2015.07.015
10. Mossadegh-Keller N, Gentek R, Gimenez G et al (2017) Developmental origin and maintenance of distinct testicular macrophage populations. J Exp Med 214:2829–2841. https://doi.org/10.1084/jem.20170829
11. Wynn TA, Chawla A, Pollard JW (2013) Macrophage biology in development, homeostasis and disease. Nature 496:445–455. https://doi.org/10.1038/nature12034
12. Cohen PE, Chisholm O, Arceci RJ et al (1996) Absence of colony-stimulating factor-1 in osteopetrotic (csfmoP/csfmOP) mice results in male fertility defects. Biol Reprod 55:310–317. https://doi.org/10.1095/biolreprod55.2.310
13. Bergh A, Damber JE, Van Rooijen N (1993) Liposome-mediated macrophage depletion: an experimental approach to study the role of testicular macrophages in the rat. J Endocrinol 136:407–413. https://doi.org/10.1677/joe.0.1360407
14. Gaytan F, Bellido C, Aguilar E, Van Rooijen N (1994) Requirement for testicular macrophages in Leydig cell proliferation and differentiation during prepubertal development in rats. J Reprod Fertil 102:393–399. https://doi.org/10.1530/jrf.0.1020393
15. Hales DB (2002) Testicular macrophage modulation of Leydig cell steroidogenesis. J Reprod Immunol 57:3–18. https://doi.org/10.1016/S0165-0378(02)00020-7
16. Hedger MP, Meinhardt A (2003) Cytokines and the immune-testicular axis. J Reprod Immunol 58:1–26. https://doi.org/10.1016/S0165-0378(02)00060-8
17. Oatley JM, Oatley MJ, Avarbock MR et al (2009) Colony stimulating factor 1 is an extrinsic stimulator of mouse spermatogonial stem cell self-renewal. Development 136:1191–1199. https://doi.org/10.1242/dev.032243
18. Kern S, Robertson SA, Mau VJ, Maddocks S (1995) Cytokine secretion by macrophages in the rat testis1. Biol Reprod 53:1407–1416. https://doi.org/10.1095/biolreprod53.6.1407
19. Rodríguez-Gil JE, Silvers G, Flores E et al (2007) Expression of the GM-CSF receptor in ovine spermatozoa: GM-CSF effect on sperm viability and motility of sperm subpopulations after the freezing-thawing process. Theriogenology 67:1359–1370. https://doi.org/10.1016/j.theriogenology.2007.02.008
20. Du Plessis SS, Agarwal A, Mohanty G, Van Der Linde M (2015) Oxidative phosphorylation versus glycolysis: what fuel do spermatozoa use? Asian J Androl 17:230–235. https://doi.org/10.4103/1008-682X.135123
21. Suarez SS (2008) Control of hyperactivation in sperm. Hum Reprod Update 14:647–657. https://doi.org/10.1093/humupd/dmn029
22. Jin SK, Yang WX (2017) Factors and pathways involved in capacitation: how are they regulated? Oncotarget 8:3600–3627. https://doi.org/10.18632/oncotarget.12274
23. Lishko PV, Kirichok Y, Ren D et al (2012) The control of male fertility by spermatozoan ion channels. Annu Rev Physiol 74:453–475. https://doi.org/10.1146/annurev-physiol-020911-153258
24. Song L, Luo ZQ (2019) Post-translational regulation of ubiquitin signaling. J Cell Biol 218:1776–1786. https://doi.org/10.1083/JCB.201902074
25. Shan J, Zhao W, Gu W (2009) Suppression of cancer cell growth by promoting cyclin D1 degradation. Mol Cell 36:469–476. https://doi.org/10.1016/j.molcel.2009.10.018
26. Gewies A, Grimm S (2003) UBP41 is a proapoptotic ubiquitin-specific protease. Cancer Res 63:682–688
27. Priolo C, Tang D, Brahamandan M et al (2006) The isopeptidase USP2a protects human prostate cancer from apoptosis. Cancer Res 66:8625–8632. https://doi.org/10.1158/0008-5472.CAN-06-1374
28. Molusky MM, Li S, Ma D et al (2012) Ubiquitin-specific protease 2 regulates hepatic gluconeogenesis and diurnal glucose

metabolism through 11b -hydroxysteroid dehydrogenase 1. Diabetes 61:1025–1035. https://doi.org/10.2337/db11-0970
29. Kitamura H, Kimura S, Shimamoto Y et al (2013) Ubiquitin-specific protease 2–69 in macrophages potentially modulates metainflammation. FASEB J 27:4940–4953. https://doi.org/10.1096/fj.13-233528
30. Hashimoto M, Saito N, Ohta H et al (2019) Inhibition of ubiquitin-specific protease 2 causes accumulation of reactive oxygen species, mitochondria dysfunction, and intracellular ATP decrement in C2C12 myoblasts. Physiol Rep 7:1–14. https://doi.org/10.14814/phy2.14193
31. Saito N, Kimura S, Miyamoto T et al (2017) Macrophage ubiquitin-specific protease 2 modifies insulin sensitivity in obese mice. Biochem Biophys Rep 9:322–329. https://doi.org/10.1016/j.bbrep.2017.01.009
32. Li C, Zhang J, Xu H et al (2018) Retigabine ameliorates acute stress-induced impairment of spatial memory retrieval through regulating USP2 signaling pathways in hippocampal CA1 area. Neuropharmacology 135:151–162. https://doi.org/10.1016/j.neuropharm.2018.02.034
33. He X, Li Y, Li C et al (2013) USP2a negatively regulates IL-1β- and virus-induced NF-κB activation by deubiquitinating TRAF6. J Mol Cell Biol 5:39–47. https://doi.org/10.1093/jmcb/mjs024
34. Kitamura H, Ishino T, Shimamoto Y et al (2017) Ubiquitin-specific protease 2 modulates the lipopolysaccharide-elicited expression of proinflammatory cytokines in macrophage-like HL-60 cells. Mediat Inflamm 2017:6909415. https://doi.org/10.1155/2017/6909415
35. Metzig M, Nickles D, Falschlehner C et al (2011) An RNAi screen identifies USP2 as a factor required for TNF-α-induced NF-κB signaling. Int J Cancer 129:607–618. https://doi.org/10.1002/ijc.26124
36. Lin H, Keriel A, Morales CR et al (2001) Divergent N-terminal sequences target an inducible testis deubiquitinating enzyme to distinct subcellular structures. Mol Cell Biol 21:977–977. https://doi.org/10.1128/mcb.21.3.977-977.2001
37. Bedard N, Yang Y, Gregory M et al (2011) Mice lacking the USP2 deubiquitinating enzyme have severe male subfertility associated with defects in fertilization and sperm motility. Biol Reprod 85:594–604. https://doi.org/10.1095/biolreprod.110.088542
38. Hasegawa Y, Daitoku Y, Sekiguchi K et al (2013) Novel ROSA26 Cre-reporter knock-in C57BL/6N mice exhibiting green emission before and red emission after Cre-mediated recombination. Exp Anim 62:295–304. https://doi.org/10.1538/expanim.62.295
39. Clausen BE, Burkhardt C, Reith W et al (1999) Conditional gene targeting in macrophages and granulocytes using LysMcre mice. Transgenic Res 8:265–277
40. Zhang X, Goncalves R, Mosser DM (2008) The isolation and characterization of murine macrophages. Curr Protoc Immunol. https://doi.org/10.1002/0471142735.im1401s83
41. Bryniarski K, Szczepanik M, Maresz K et al (2004) Subpopulations of mouse testicular macrophages and their immunoregulatory function. Am J Reprod Immunol 52:27–35. https://doi.org/10.1111/j.1600-0897.2004.00178.x
42. Handel-Fernandez ME, Ilkovitch D, Iragavarapu-Charyulu V et al (2009) Decreased levels of both Stat1 and Stat3 in T lymphocytes from mice bearing mammary tumors. Anticancer Res 29:2051–2058
43. Metsalu T, Vilo J (2015) ClustVis: a web tool for visualizing clustering of multivariate data using principal component analysis and heatmap. Nucleic Acids Res 43:W566–W570. https://doi.org/10.1093/nar/gkv468
44. Yanagawa Y, Matsuura Y, Suzuki M et al (2015) Accessory corpora lutea formation in pregnant hokkaido sika deer (Cervus nippon yesoensis) investigated by examination of ovarian dynamics and steroid hormone concentrations. J Reprod Dev 61:61–66. https://doi.org/10.1262/jrd.2014-076
45. Kanno C, Sakamoto KQ, Yanagawa Y et al (2017) Comparison of sperm subpopulation structures in first and second ejaculated semen from Japanese black bulls by a cluster analysis of sperm motility evaluated by a CASA system. J Vet Med Sci 79:1359–1365. https://doi.org/10.1292/jvms.17-0012
46. Wang WH, Abeydeera LR, Fraser LR, Niwa K (1995) Functional analysis using chlortetracycline fluorescence and in vitro fertilization of frozen–thawed ejaculated boar spermatozoa incubated in a protein-free chemically defined medium. J Reprod Fertil 104:305–313. https://doi.org/10.1530/jrf.0.1040305
47. Schneider CA, Rasband WS, Eliceiri KW (2012) NIH Image to ImageJ: 25 years of image analysis. Nat Methods 9:671–675. https://doi.org/10.1038/nmeth.2089
48. Peer NR, Law SM, Murdoch B et al (2018) Germ cell–specific retinoic acid receptor a functions in germ cell organization, meiotic integrity, and spermatogonia. Endocrinology 159:3403–3420. https://doi.org/10.1210/en.2018-00533
49. Vernet N, Dennefeld C, Guillou F et al (2006) Prepubertal testis development relies on retinoic acid but not rexinoid receptors in Sertoli cells. EMBO J 25:5816–5825. https://doi.org/10.1038/sj.emboj.7601447
50. Abram McBride J, Lipshultz L (2018) Male fertility preservation. Curr Urol Rep 19:49. https://doi.org/10.1007/s11934-018-0803-2
51. Morrell JM, Mayer I (2017) Reproduction biotechnologies in germplasm banking of livestock species: a review. Zygote 25:545–557. https://doi.org/10.1017/S0967199417000442
52. Comizzoli P (2015) Biobanking efforts and new advances in male fertility preservation for rare and endangered species. Asian J Androl 17:640–645. https://doi.org/10.4103/1008-682X.153849
53. Matamoros-Volante A, Treviño CL (2020) Capacitation-associated alkalization in human sperm is differentially controlled at the subcellular level. J Cell Sci 133:jcs238816. https://doi.org/10.1242/jcs.238816
54. Gruschwitz MS, Brezinschek R, Brezinschek HP (1996) Cytokine levels in the seminal plasma of infertile males. J Androl 17:158–163
55. Bernabò N, Di AR, Ordinelli A et al (2016) The maturation of murine spermatozoa membranes within the epididymis, a computational biology perspective. Syst Biol Reprod Med 62:299–308. https://doi.org/10.1080/19396368.2016.1205679
56. Smith TB, Cortez-Retamozo V, Grigoryeva LS et al (2014) Mononuclear phagocytes rapidly clear apoptotic epithelial cells in the proximal epididymis. Andrology 2:755–762. https://doi.org/10.1111/j.2047-2927.2014.00251.x
57. Da Silva N, Smith TB (2015) Exploring the role of mononuclear phagocytes in the epididymis. Asian J Androl 17:591–596. https://doi.org/10.4103/1008-682X.153540
58. Shum WW, Smith TB, Cortez-Retamozo V et al (2014) Epithelial basal cells are distinct from dendritic cells and macrophages in the mouse epididymis. Biol Reprod 90:1–10. https://doi.org/10.1095/biolreprod.113.116681
59. Padilla L, Martínez-Hernández J, Barranco I et al (2020) Granulocyte-macrophage colony stimulating factor (GM-CSF) is fully expressed in the genital tract, seminal plasma and spermatozoa of male pigs. Sci Rep 10:1–12. https://doi.org/10.1038/s41598-020-70302-9
60. Turner RM (2006) Moving to the beat: a review of mammalian sperm motility regulation. Reprod Fertil Dev 18:25–38. https://doi.org/10.1071/RD05120
61. Loveland KL, Klein B, Pueschl D et al (2017) Cytokines in male fertility and reproductive pathologies: immunoregulation and beyond. Front Endocrinol (Lausanne) 8:1–16. https://doi.org/10.3389/fendo.2017.00307

62. Eisermann J, Register K, Strickler R, Collins J (1989) The Effect of tumor necrosis factor on human sperm motility in vitro. J Androl 10:270–274. https://doi.org/10.1002/j.1939-4640.1989.tb00100.x
63. Ganaiem M, AbuElhija M, Lunenfeld E et al (2009) Effect of interleukin-1 receptor antagonist gene deletion on male mouse fertility. Endocrinology 150:295–303. https://doi.org/10.1210/en.2008-0848
64. Isobe T, Minoura H, Tanaka K et al (2002) The effect of RANTES on human sperm chemotaxis. Hum Reprod 17:1441–1446. https://doi.org/10.1093/humrep/17.6.1441
65. Naz R, Kaplan P (1994) Interleukin-6 enhances the fertilizing capacity of human sperm by increasing capacitation and acrosome reaction. J Androl 15:228–233. https://doi.org/10.1002/j.1939-4640.1994.tb00438.x
66. McLay RN, Banks WA, Kastin AJ (1997) Granulocyte macrophage-colony stimulating factor crosses the blood-testis barrier in mice. Biol Reprod 57:822–826. https://doi.org/10.1095/biolreprod57.4.822
67. Zambrano A, Noli C, Rauch MC et al (2001) Expression of GM-CSF receptors in male germ cells and their role in signaling for increased glucose and vitamin C transport. J Cell Biochem 80:625–634. https://doi.org/10.1002/1097-4644(20010315)80:4%3c625::AID-JCB1017%3e3.0.CO;2-9
68. Vilanova LT, Rauch MC, Mansilla A, Werner E (2003) Expression of granulocyte–macrophage colony stimulating factor (GM-CSF) in male germ cells : GM-CSF enhances sperm motility. Theriogenology 60:1083–1095. https://doi.org/10.1016/S0093-691X(03)00106-7
69. Leu JIJ, Barnoud T, Zhang G et al (2017) Inhibition of stress-inducible HSP70 impairs mitochondrial proteostasis and function. Oncotarget 8:45656–45669. https://doi.org/10.18632/oncotarget.17321
70. Calle-Guisado V, Bragado MJ, García-Marín LJ, González-Fernández L (2017) HSP90 maintains boar spermatozoa motility and mitochondrial membrane potential during heat stress. Anim Reprod Sci 187:13–19. https://doi.org/10.1016/j.anireprosci.2017.09.009
71. Al-Shami A, Mahanna W, Naccache PH (1998) Granulocyte-macrophage colony-stimulating factor-activated signaling pathways in human neutrophils. J Biol Chem 273:1058–1063. https://doi.org/10.1074/jbc.273.2.1058
72. Stephanou A, Latchman DS (1999) Transcriptional regulation of the heat shock protein genes by STAT family transcription factors. Gene Exp 7:311–319
73. Ward CR, Storey BT (1984) Determination of the time course of capacitation in mouse spermatozoa using a chlortetracycline fluorescence assay. Dev Biol 104:287–296. https://doi.org/10.1016/0012-1606(84)90084-8
74. Liu YX (2007) Involvement of plasminogen activator and plasminogen activator inhibitor type 1 in spermatogenesis, sperm capacitation, and fertilization. Semin Thromb Hemost 33:29–40. https://doi.org/10.1055/s-2006-958459
75. Ebisch IMW, Steegers-Theunissen RPM, Sweep FCGJ et al (2007) Possible role of the plasminogen activation system in human subfertility. Fertil Steril 87:619–626. https://doi.org/10.1016/j.fertnstert.2006.07.1510
76. Cabrillana ME, Monclus MDLÁ, Lancellotti TES et al (2017) Thiols of flagellar proteins are essential for progressive motility in human spermatozoa. Reprod Fertil Dev 29:1435–1446. https://doi.org/10.1071/RD16225
77. Dirami G, Poulter LW, Cooke BA (1991) Separation and characterization of Leydig cells and macrophages from rat testes. J Endocrinol 130:357–365. https://doi.org/10.1677/joe.0.1300357
78. Cudicini C, Lejeune H, Gomez E et al (1997) Human leydig cells and sertoli cells are producers of interleukins-1 and-6. J Clin Endocrinol Metab 82:1426–1433. https://doi.org/10.1210/jcem.82.5.3938
79. Gérard N, Syed V, Bardin W et al (1991) Sertoli cells are the site of interleukin-1α synthesis in rat testis. Mol Cell Endocrinol 82:13–16. https://doi.org/10.1016/0303-7207(91)90019-O
80. Bou Ghosn EE, Cassado AA, Govoni GR et al (2010) Two physically, functionally, and developmentally distinct peritoneal macrophage subsets. Proc Natl Acad Sci USA 107:2568–2573. https://doi.org/10.1073/pnas.0915000107
81. White SL, Belov L, Barber N et al (2005) Immunophenotypic changes induced on human HL60 leukaemia cells by 1α,25-dihydroxyvitamin D3 and 12-O-tetradecanoyl phorbol-13-acetate. Leuk Res 29:1141–1151. https://doi.org/10.1016/j.leukres.2005.02.012
82. Cockerill GW, Bert AG, Ryan GR et al (1995) Regulation of granulocyte-macrophage colony-stimulating factor and E- selectin expression in endothelial cells by cyclosporin A and the T-cell transcription factor NFAT. Blood 86:2689–2698. https://doi.org/10.1182/blood.v86.7.2689.2689
83. Schreck R, Baeuerle PA (1990) NF-kB inducible transcriptional activator of the granulocyte- macrophage colony-stimulating factor gene. Mol Cell Biol 10:1281–1286
84. Ghiorzo P, Musso M, Mantelli M et al (1997) C-Rel and p65 subunits bind to an upstream NF-κB site in human granulocyte macrophage-colony stimulating factor promoter involved in phorbol ester response in 5637 cells. FEBS Lett 418:215–218. https://doi.org/10.1016/S0014-5793(97)01387-2
85. Yang TC, Chang PY, Kuo TL, Lu SC (2017) Electronegative L5-LDL induces the production of G-CSF and GM-CSF in human macrophages through LOX-1 involving NF-κB and ERK2 activation. Atherosclerosis 267:1–9. https://doi.org/10.1016/j.atherosclerosis.2017.10.016
86. Seiler P, Cooper TG, Yeung CH, Nieschlag E (1999) Regional variation in macrophage antigen expression by murine epididymal basal cells and their regulation by testicular factors. J Androl 20:738–746. https://doi.org/10.1002/j.1939-4640.1999.tb03379.x
87. Da Silva N, Barton CR (2016) Macrophages and dendritic cells in the post-testicular environment. Cell Tissue Res 363:97–104. https://doi.org/10.1007/s00441-015-2270-0
88. Ge W, Yue Y, Xiong S (2019) POM121 inhibits the macrophage inflammatory response by impacting NF-κB P65 nuclear accumulation. Exp Cell Res 377:17–23. https://doi.org/10.1016/j.yexcr.2019.02.021
89. Wang Y, Dong G, Jeon HH et al (2015) FOXO1 mediates RANKL-induced osteoclast formation and activity. J Immunol 194:2878–2887. https://doi.org/10.4049/jimmunol.1402211
90. Zhang Y, Xu S, Li K et al (2017) mTORC1 inhibits NF-κB/NFATc1 signaling and prevents osteoclast precursor differentiation, in vitro and in mice. J Bone Miner Res 32:1829–1840. https://doi.org/10.1002/jbmr.3172
91. Orthgiess J, Gericke M, Immig K et al (2016) Neurons exhibit Lyz2 promoter activity in vivo: Implications for using LysM-Cre mice in myeloid cell research. Eur J Immunol 46:1529–1532. https://doi.org/10.1002/eji.201546108